Diffusive transport in networks built of containers and tubes

L. Lizana and Z. Konkoli*
Department of Applied Physics, Chalmers University of Technology and Göteborg University, SE-412 96 Göteborg, Sweden
(Received 11 March 2005; published 25 August 2005)

We have developed analytical and numerical methods to study the transport of noninteracting particles in large networks consisting of M d-dimensional containers $C_1,\ldots,C_M$ with radii R_i linked together by tubes of length l_{ij} and radii a_{ij} where $i,j=1,2,\ldots,M$. Tubes may join directly with each other, forming junctions. It is possible that some links are absent. Instead of solving the diffusion equation for the full problem we formulated an approach that is computationally more efficient. We derived a set of rate equations that govern the time dependence of the number of particles in each container, $N_1(t),N_2(t),\ldots,N_M(t)$. In such a way the complicated transport problem is reduced to a set of M first-order integro-differential equations in time, which can be solved efficiently by the algorithm presented here. The workings of the method have been demonstrated on a couple of examples: networks involving three, four, and seven containers and one network with a three-point junction. Already simple networks with relatively few containers exhibit interesting transport behavior. For example, we showed that it is possible to adjust the geometry of the networks so that the particle concentration varies in time in a wavelike manner. Such behavior deviates from simple exponential growth and decay occurring in the two-container system.

DOI: 10.1103/PhysRevE.72.026305 PACS number(s): 89.75.Hc, 05.40.−a

I. INTRODUCTION

The goal of this work is to find a method that describes the diffusive transport of particles on a network built up of spherical containers connected by tubes. It is possible that not all containers are connected to each other and tubes may join together, forming junctions (without a container being present). In such a way one can generate an enormous number of network topologies. One example is shown in Fig. 1. The networks consists of M containers (reservoirs) labeled $C_1,\ldots,C_M$ of radii R_i connected by tubes of length l_{ij} and radii a_{ij} where $i,j=1,2,\ldots,M$.

Our work is motivated by experiments discussed in Refs. [1–3] and [4–6]. The first set of references describes how to create and manipulate microscale-sized compartments (vesicles) connected by nanotubes. These structures can be applied in a number of ways [3]. For example, nondiffusive (forced) transport was studied in [1]. In this work we study different kinds of transport where only passive diffusion is allowed. Also, by including the reactions in the theoretical setup one could describe biochemical reactions in a milieu close to their natural habitat. This idea was pursued experimentally in Ref. [2].

The second set of references deals with networks of chemical reactors of macroscopic sizes connected to each other by tubes. The exchange of reactants is mediated through the tubes and controlled by pumps. It was shown that it is possible to use this device to carry out pattern recognition tasks. In making the device smaller the external pumping can be removed and the transport can be limited to pure diffusion. This kind of setup is close to the situation studied here.

For large networks, links connecting opposite sides of the network may be rather long. Accordingly, one cannot expect an exponential decay of the number of particles in the containers and this is the situation we are mostly interested in. Obviously, to describe such a situation one can attempt to solve the diffusion equation numerically and obtain the distribution function $\rho(\vec{r},t)$ that describes how particles spread throughout the network.

Obtaining the solution of the diffusion equation for a complicated geometry for a large networks gets highly impractical. In this work we develop a method of calculation that is computationally efficient and can be used to study transport in large networks. Instead of finding the full distribution function $\rho(\vec{r},t)$ we introduce a set of slow variables that capture the most important aspect of particle transport, the number of particles in each container $N_1(t),N_2(t),\ldots,N_M(t)$, and derive equations that describe how they change in time. This is the central result of the paper.

A couple of related problems have been addressed previously in Refs. [7–11]. Escape of a particle through a small hole in a cavity was studied in [7]. The work of [8] deals with the problem of a hole connected to a short tube. The tube length and hole radius are roughly of the same size,

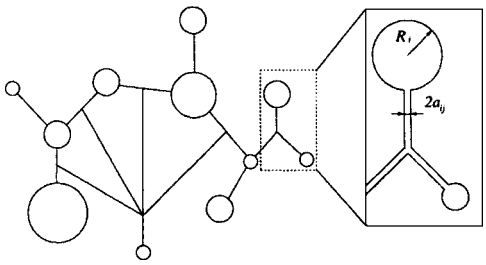

FIG. 1. Schematic picture of an arbitrary network built from containers and tubes.

*FAX: +46 31 41 69 84. Electronic address: zorank@fy.chalmers.se

mimicking a cell membrane having a thickness greater than zero. A couple of equilibration cases have also been studied [9–11]. The papers just indicated treat the intracontainer dynamics in much more detail than we do. Here, for simplicity reasons, the particle concentration is assumed flat in the container and the validity of this approximation is checked numerically in Sec. VII. In our notation, the studies [7–11] can be classified as $M=1,2$ cases. Our main interest is in networks with large M.

This paper is organized as follows. In Sec. II the problem is defined and the general results are stated. The derivation of the rate equation given in Eq. (3), is explained in Secs. III and IV where the emptying of a single container into a tube and the emptying of a container into another container through the tube are studied. The single-exponential asymptotics of the two-container system and related first-order rate equations are found and discussed in Sec. V. Up to this point only a two-container system is treated while Sec. VI deals with an arbitrary network topology. Section VII elaborates on the assumption of well-stirred containers. A numerical comparison to the diffusion equation is made. In Sec. VIII numerical case studies of various network structures are performed. In particular a three-way junction and an example of a larger network are studied. The summary and outline of future work is given in Sec. IX. Technical details are found in the Appendixes. Appendix A describes the numerical procedure used for solving the rate equations. The rate equations for the cases studied in Sec. VIII are explicitly derived in Appendix C. It can be shown that the presence of tube junctions can be eliminated altogether from the dynamical equations when the time is large. This is demonstrated in Appendix D.

II. PROBLEM DEFINITION AND MAIN RESULT

Describing the particle transport in a network depicted in Fig. 1 is far from trivial, and in order to solve the problem several assumptions are made. We assume that (i) particles move solely by diffusion (the fluid in which the particles move stands still) and (ii) particles do not disturb each other. With these assumptions the complicated dynamical problem at hand is reduced to solving the time-dependent diffusion equation

$$\partial_t \rho(\vec{r},t) = \vec{\nabla}\cdot[D(\vec{r})\vec{\nabla}\rho(\vec{r},t)]. \tag{1}$$

Here $\rho(\vec{r},t)$ is the concentration (particle density) and $D(\vec{r})$ is the diffusion coefficient which may be position dependent. The walls are particle impenetrable,

$$\partial_n \rho(\vec{r},t) = 0, \tag{2}$$

where $\partial_n \equiv \hat{n}\cdot\vec{\nabla}$ and $\hat{n}$ is the unit vector perpendicular to the wall. The total number of particles is a conserved quantity.

Equation (1) could in principle be solved numerically using a brute force approach (e.g., the finite-element method or the finite-difference method). However, in Secs. III and IV we will show that it is possible to describe particle transport in terms of a finite number of variables, the number of particles in each container, $N_1,\ldots,N_M$. Also, it might be easier to understand particle transport in such a setup. The dynamics of $N_i(t)$, $i=1,\ldots,M$, is governed by

$$\dot{N}_i(t) = \sum_{j=1}^{M} \mathcal{C}_{ji}\frac{V_{d-1}(a_{ji})}{V_d(R_j)}\int_0^t dt'\mathcal{N}_j(t')\sigma_{ji}(t-t') - \sum_{j=1}^{M}\mathcal{C}_{ij}\frac{V_{d-1}(a_{ij})}{V_d(R_i)}\int_0^t dt'\mathcal{N}_i(t')[\Delta_{ij}(t-t')+\kappa_{ij}(t-t')], \tag{3}$$

where

$$\mathcal{N}_i(t) \equiv \dot{N}_i(t) + N_{i0}\delta(t) \tag{4}$$

and $\delta(t)$ is the Dirac delta function, $\int_0^\infty dt\,\delta(t)=1$. Here and in the following the overdot denotes time derivative. The connectivity matrix $\mathcal{C}_{ij}\in\{0,1\}$ describes how the nodes are linked (note that $\mathcal{C}_{ii}=0$), a_{ij} is the radius of the tube (link) from i to j, and $V_d(R_j)$ is the volume of a d-dimensional sphere, $V_d(r)=[2\pi^{d/2}/d\Gamma(d/2)]r^d$, corresponding to container j having radius R_j. N_{i0} denotes $N_i(t=0)$. Equation (3) is derived under the assumption of ideally mixed containers. The rate coefficients are given by

$$\Delta_{ij}(t) = \sqrt{\frac{D_{ij}}{\pi t}},$$

$$\kappa_{ij}(t) = 2\sqrt{\frac{D_{ij}}{\pi t}}\sum_{k=1}^{\infty}\exp\left(-\frac{(k\ell_{ij})^2}{D_{ij}t}\right),$$

$$\sigma_{ij}(t) = 2\sqrt{\frac{D_{ij}}{\pi t}}\sum_{k=0}^{\infty}\exp\left(-\frac{((2k-1)\ell_{ij})^2}{4D_{ij}t}\right). \tag{5}$$

ℓ_{ij} is the link length, and D_{ij} is the corresponding diffusion coefficient. The theory is developed for the general case where the diffusion constant in each tube may be different.

Figure 1 also shows the existence of tube junctions. They are treated by Eq. (3) by letting the container radius coincide with that of the tube. Since the tubes are initially empty, so are the junctions, $N_{i0}=0$. Equations (3)–(5) are the central results of this paper, and their derivation is a major topic of the subsequent sections.

III. EMPTYING OF A RESERVOIR THROUGH AN INFINITELY LONG TUBE

To derive Eq. (3) we start with the simplest possible case and consider particle escape from a container through an infinitely long tube [see Fig. 2(a)]. The main reason for this is to show how to couple the dynamics of the tube and container. Also, such a setup captures the short-time description of the full network problem when the particles escaping the containers do not yet "feel" that the system is closed [the short-time dynamics is contained in $\Delta(t)$; see Sec. IV].

The particle concentration $\rho(\vec{r},t)$ is governed by the diffusion equation supplemented with the boundary conditions that the walls be impenetrable and that $\rho(\vec{r},t)$ vanish for x

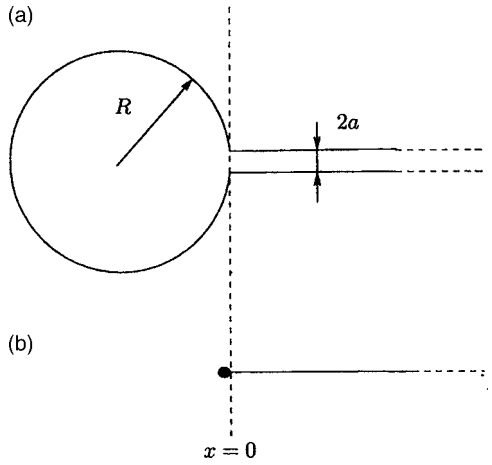

FIG. 2. (a) A spherical compartment connected to a cylindrical infinitely long tube. If the tube radius is assumed to be small, the compartment can be treated as ideally mixed at all times, simplifying the dynamics in the container. The transport in the tube is reduced to a one-dimensional diffusion problem. Panel (b) illustrates these simplifications.

$\rightarrow\infty$. The concentrations in the tube and container are interwoven in a highly nontrivial way through what is occurring at the tube opening. Given that the current density out of the container $j(0,y,z,t)$ is known [see Fig. 2(a)] one could solve the diffusion problem and find the concentration profile in the container and the number of particles. Furthermore, one could find a relationship

$$\rho(0^-,y,z,t) = \mathcal{F}[j(0,y,z,t)], \tag{6}$$

where $j(0,y,z,t) = -D \lim_{x\to 0^-} \hat{x}\cdot\vec{\nabla}\rho(x,y,z,t)$. $\mathcal{F}$ is a functional that we know exists but is unlikely to be found in a closed analytic form.

To find $j(0,y,z,t)$ it is assumed that the concentration in the vicinity of the tube opening can be approximated by

$$\rho(x,y,z,t) = f(y,z,t)c(x,t), \quad x \gtrsim 0, \tag{7}$$

where $c(x,t)$ is a one-dimensional concentration and $f(z,y,t)$ is a function that projects the value of $c(x,t)$ onto a radial direction. Equation (7) is valid for large x when $f(y,z,t)$ is constant but not in the general case. The arbitrary density profile at the opening will in time smear out due to radial diffusion.

By assumption, the concentration profile in the tube is governed by $c(x,t)$ and it is coupled to the concentration in the container as follows. Both concentration and current have to be continuous as one moves from the container into the tube, leading to

$$\rho(0,y,z,t) = f(y,z,t)c(0,t) \tag{8}$$

and

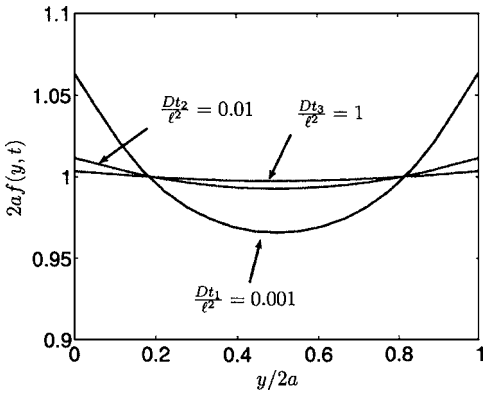

FIG. 3. Behavior of $f(y,z,t)$ defined in Eq. (7) for the two-dimensional system shown in Fig. 9 [panel (a), $a/R=0.1$] at three different instants of time $t_1<t_2<t_3$. The graph verifies the assumption that $f(y,z,t)$ is approximately constant. In this two-dimensional case $f(y,t)\rightarrow 1/2a$ as $t\rightarrow\infty$.

$$j(0,y,z,t) = f(y,z,t)\lim_{x\to 0^+}\frac{\partial}{\partial x}c(x,t). \tag{9}$$

Note that $\lim_{x\to 0^+}(\partial/\partial x)c(x,t)$ in Eq. (9) is a functional of $c(0,t)$. Taking into account particle conservation at the tube opening leads to

$$\int_{x=0} dS\rho(0,y,z,t) = c(0,t), \tag{10}$$

which after using Eq. (8) results in the condition $\int dSf(y,z,t)=1$. The problem has four unknowns $\rho(0,y,z,t)$, $j(0,y,z,t)$, $c(0,t)$, and $f(y,z,t)$ and four equations (6) and (8)–(10) and is fully defined. However, it is not tractable in this complicated form and we proceed to simplify it.

Instead of $\rho(\vec{r},t)$ a more useful variable is the total number of particles in the container $N(t)=\int_{x<0} dV\rho(\vec{r},t)$ governed by

$$\dot{N}(t) = -J(t), \tag{11}$$

where $J(t)$ is the flow of particles that leave the container through the tube opening $J(t)=\int dSj(0,y,z,t)$. There are two special cases where the current $J(t)$ can be determined analytically in terms of container variables. (i) If the exit is a fully absorbing disk with radius a, the concentration is always zero at the the interface $\rho(0,y,z,t)=0$. In [12] it is shown that the current J_∞ through such a disk when placed at an infinite otherwise reflecting wall is $J_\infty=4D_c a\rho_\infty$ where ρ_∞ is the particle concentration at infinity and D_c denotes the diffusion constant in the container. A reasonable assumption for the container, at least when the tube radius is smaller than the radius of the container, is that the concentration profile far away from the exit is flat and can approximately be taken to be $N(t)/V_d(R)$. Using this for ρ_∞ yields $J_\infty(t)=4D_c aN(t)/V_d(R)$. (ii) If the opening is completely closed, the current is zero and $\rho(0,y,z,t)=N(t)/V_d(R)$ [in such a case $N(t)=N(0)$]. A linear interpolation between (i) and (ii) yields

$$\rho(0,y,z,t) = \frac{N(t)}{V_d(R)}\left[1 - \frac{J(t)}{J_\infty(t)}\right]. \tag{12}$$

Note that, in Eq. (12), $\rho(0,y,z,t)$ is assumed constant across the interface. This approximation is verified numerically in Fig. 3, which shows $f(y,z,t) \approx V_{d-1}(a)^{-1}$. Also, when $a \ll R$ one has $J(t)/J_\infty(t) \ll 1$ and second term in Eq. (12) can be neglected. This approximation is verified by numerical calculations in Sec. VII.

At this point, the full problem has been mapped onto a very simple geometry depicted in Fig. 2(b): a one-dimensional line (tube) connected to a point (container). The tube dynamics is characterized by a one-dimensional particle density $c(x,t)$ along the line, and all container dynamics, how complicated it may be, has been projected on to a single variable $N(t)$.

The only part of the problem that remains to be solved is the diffusion through the tube. This part of the problem can be approximated by one-dimensional diffusion since $f(y,z,t)$ is constant. The constant concentration profile at the tube opening remains such in the tube interior (provided the tube radius does not change along the x direction). With the assumptions at hand the coupling Eq. (8) becomes

$$c(0,t) = V_{d-1}(a)\frac{N(t)}{V_d(R)}. \tag{13}$$

The concentration profile along the tube [initially empty $c(x,0)=0$] is given by the diffusion equation

$$\frac{\partial c(x,t)}{\partial t} = D\frac{\partial^2 c(x,t)}{\partial x^2}, \quad x \in [0,\infty), \tag{14}$$

supplemented with boundary conditions according to Eq. (13) and $c(\infty,t)=0$. The solution can be found by the Laplace transform method [13] and is given by

$$c(x,s) = c(0,s)e^{-x\sqrt{s/D}}, \tag{15}$$

where $c(x,s)=\int_0^\infty dt c(x,t)e^{-st}$. Integrating Eq. (9) over the tube interface area at $x=0$ gives

$$J(t) = -D\lim_{x\to 0}\frac{\partial}{\partial x}c(x,t). \tag{16}$$

Combining Eqs. (11), (13), and (16) leads to a rate equation in the Laplace transform space:

$$\begin{aligned} sN(s) - N_0 &= -\lim_{x\to 0}\sqrt{sD}N(s)\frac{V_{d-1}(a)}{V_d(R)}e^{-x\sqrt{s/D}} \\ &= -\sqrt{sD}N(s)\frac{V_{d-1}(a)}{V_d(R)}, \end{aligned} \tag{17}$$

where $\mathcal{L}[\dot{N}(t)]=sN(s)-N_0$. It is tempting to rewrite this equation in the time domain in the form of a convolution,

$$\dot{N}(t) = -\int_0^t dt' k(t')N(t-t'), \tag{18}$$

representing a general form of a rate law, where $k(t) = [V_{d-1}(a)/V_d(R)]\mathcal{L}^{-1}[\sqrt{Ds}]$. However, this is impossible and can be seen in several ways.

First, $\sqrt{s}$ has no well-defined inverse Laplace transform and $k(t)$, which would enter into the rate equation (18), is ill defined. Second, this problem could possibly be resolved by inverting Eq. (15) to obtain $c(x,t)$ and inserting the result into Eq. (16) which leads to

$$J(t) \propto -\lim_{x\to 0}\frac{\partial}{\partial x}\int_0^t dt' \frac{x}{t'^{3/2}}e^{-x^2/4Dt'}N(t-t'). \tag{19}$$

In general $N(t)$ is unknown. To evaluate the expression above in a way that would result in a rate equation involves interchanging derivation and integration. This is only allowed if the integral is uniformly convergent in the interval $x \in [0,\infty)$ [14]. It is easy to see from Eq. (19) that this is not the case and the interchange is illegal. Another possibility is to use partial integration but this strategy does not work since one ends up with nonconvergent integrals as $x\to 0$. Thus, Eq. (18) does not exist for the semi-infinite case. Also, it is intuitively clear that one cannot observe pure exponential decay since the system is infinite.

For an infinite system an asymptotic rate law of the type $\dot{N}(t) \propto -N(t)$ simply does not exist. This can also be seen from the exact expression for $N(t)$ which can be obtained from Eq. (17) by solving for $N(s)$ and finding the inverse Laplace transform [13]:

$$N(t) = N_0 \exp\left[Dt\left(\frac{V_{d-1}(a)}{V_d(R)}\right)^2\right]\mathrm{erfc}\left[\sqrt{Dt}\frac{V_{d-1}(a)}{V_d(R)}\right]. \tag{20}$$

N_0 is the initial number of particles in the container. Using approximation

$$\mathrm{erfc}(z) \approx \frac{e^{-z^2}}{\sqrt{\pi}}\frac{1}{z}$$

for large z gives $N(t) \propto 1/\sqrt{t}$.

Due to the complications discussed above, the rate equation has to be stated in terms of $\dot{N}(t)$:

$$\begin{aligned} \dot{N}(t) &= -\frac{V_{d-1}(a)}{V_d(R)}\mathcal{L}^{-1}\left[sN(s)\sqrt{\frac{D}{s}}\right] \\ &= -\frac{V_{d-1}(a)}{V_d(R)}\int_0^t dt' \mathcal{N}(t')\Delta(t-t'), \end{aligned} \tag{21}$$

where

$$\mathcal{N}(t) \equiv \mathcal{L}^{-1}[sN(s)] = \dot{N}(t) + N_0\delta(t) \tag{22}$$

and

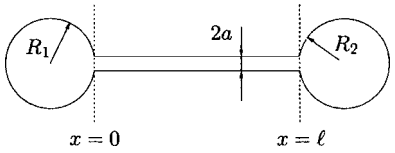

FIG. 4. Schematic picture of a two-node network.

$$\Delta(t) \equiv \mathcal{L}^{-1}\left[\sqrt{\frac{D}{s}}\right] = \sqrt{\frac{D}{\pi t}}. \tag{23}$$

Note that it is impossible to rewrite the right-hand side of Eq. (21) in such a way that it would solely involve a dependence on $N(t)$. When the system is closed (e.g., by adding another container) the situation changes.

IV. RATE EQUATION FOR A TWO-CONTAINER SYSTEM

The system under consideration consists of a one-dimensional rod parametrized by a and ℓ connected to two ideally mixed containers having radii R_1 and R_2, depicted in Fig. 4.

The diffusion equation for the tube [initially empty, $c(x,t)=0$] connected to the two containers at $x=0$ and $x=\ell$ is given by

$$\frac{\partial c(x,t)}{\partial t} = D\frac{\partial^2 c(x,t)}{\partial x^2}, \quad x \in (0,\ell), \tag{24}$$

with boundary conditions analogous to Eq. (13):

$$c(0,t) = N_1(t)\frac{V_{d-1}(a)}{V_d(R_1)}, \quad c(\ell,t) = N_2(t)\frac{V_{d-1}(a)}{V_d(R_2)}. \tag{25}$$

The solution in Laplace transform space is given by

$$c(x,s) = \frac{V_{d-1}(a)}{V_d(R_1)}sN_1(s)\phi_1(x,s) + \frac{V_{d-1}(a)}{V_d(R_2)}sN_2(s)\phi_2(x,s), \tag{26}$$

where

$$\phi_1(x,s) = \frac{\sinh((x-\ell)\sqrt{s/D})}{s\sinh(\ell\sqrt{s/D})}, \quad \phi_2(x,s) = \frac{\sinh(x\sqrt{s/D})}{s\sinh(\ell\sqrt{s/D})}. \tag{27}$$

Matching the current at both ends as in Eq. (16),

$$\dot{N}_1(t) = D\lim_{x\to 0}\frac{\partial}{\partial x}c(x,t),$$

$$\dot{N}_2(t) = -D\lim_{x\to \ell}\frac{\partial}{\partial x}c(x,t), \tag{28}$$

yields a set of rate equations in Laplace transform space for the two-container system:

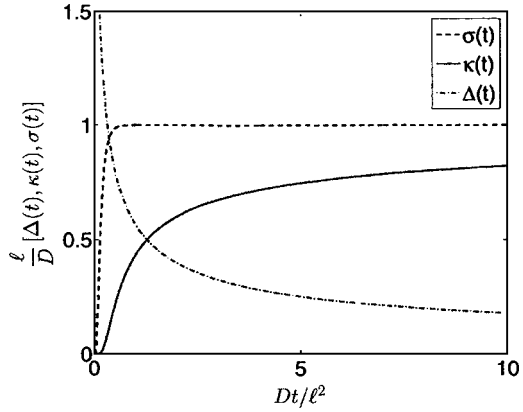

FIG. 5. Time dependence of the rate coefficients $\Delta(t)$, $\kappa(t)$, and $\sigma(t)$ from Eq. (3).

$$sN_1(s) - N_{10} = -sN_1(s)\frac{V_{d-1}(a)}{V_d(R_1)}\sqrt{\frac{D}{s}}\frac{\cosh(\ell\sqrt{s/D})}{\sinh(\ell\sqrt{s/D})} + sN_2(s)\frac{V_{d-1}(a)}{V_d(R_2)}\sqrt{\frac{D}{s}}\frac{1}{\sinh(\ell\sqrt{s/D})}, \tag{29a}$$

$$sN_2(s) - N_{20} = -sN_2(s)\frac{V_{d-1}(a)}{V_d(R_2)}\sqrt{\frac{D}{s}}\frac{\cosh(\ell\sqrt{s/D})}{\sinh(\ell\sqrt{s/D})} + sN_1(s)\frac{V_{d-1}(a)}{V_d(R_1)}\sqrt{\frac{D}{s}}\frac{1}{\sinh(\ell\sqrt{s/D})}. \tag{29b}$$

The terms having minus signs are the outflow while the ones having plus signs represent the inflow. A closer look at the the rate equations above reveals an important link to the semi-infinite case: the outflow is proportional to $\sqrt{s}$ for large t (small s). In other words, the semi-infinite case is recovered as a short-time expansion of Eqs. (29) (see Sec. III). The physical interpretation is that, initially, the particles feel as if they were entering an infinitely long tube. This implies that the outflow term can be divided into two parts reflecting this observation:

$$\sqrt{\frac{D}{s}}\left[\frac{\cosh(\ell\sqrt{s/D})}{\sinh(\ell\sqrt{s/D})}\right] \equiv \Delta(s) + \kappa(s). \tag{30}$$

$\Delta(s)$ is taken from Eq. (23) and controls the short-time dynamics that resembles the one of the semi-infinite system. $\kappa(s)$ describes the asymptotic long-time behavior when the particles are "aware" of the existence of another side and can be found from Eqs. (23) and (30):

$$\kappa(s) = \sqrt{\frac{D}{s}}\frac{\exp(-\ell\sqrt{s/D})}{\sinh(\ell\sqrt{s/D})}. \tag{31}$$

The inflow rate is labeled $\sigma(s)$:

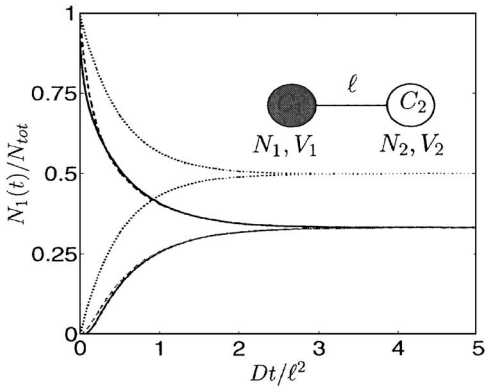

FIG. 6. The solution of Eq. (35) (solid line) is compared with a solution of Eq. (55) (dashed line). The solution of Eq. (45), given in Eq. (49), is represented by the dotted line. The curves decaying and growing describe $N_1(t)$ and $N_2(t)$, respectively. The network structure is shown in the inset. The volumes of the tube and containers are equal and $a/\ell=0.05$. The initial distribution of particles is $N_1(0)/N_{tot}=1$ and $N_2(0)/N_{tot}=0$, where $N_{tot}=N_1(0)+N_2(0)$, indicated by the shading in the inset. This figure clearly shows that Eq. (49) does not lead to the correct values for $N_1(t)$ and $N_2(t)$. The agreement with Eq. (55) is much better.

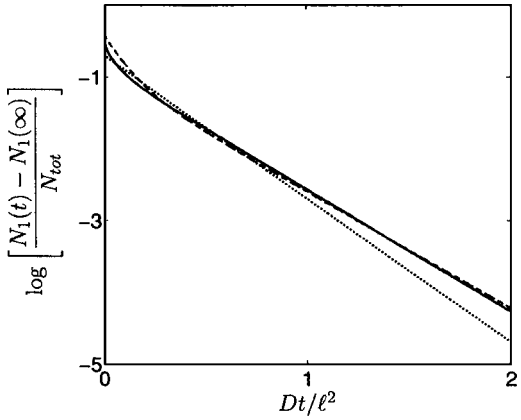

FIG. 7. The natural logarithm of $[N_1(t)-N_1(\infty)]/N_{tot}$ for the three cases illustrated in Fig. 6. The labeling of the curves is the same as in Fig. 6. The linear behavior is evidence of the single-exponential decay of the number of particles in container C_1. The slope gives the value of the decay exponent. The slopes of the solid and dashed lines are close to each other, showing that Eq. (55) is capable of estimating the decay exponent well. The slope of the dotted line differs significantly from the others which illustrates that Eq. (49) cannot describe the dynamics in an adequate way. Since the value of $N_1(\infty)$ is not the same as in all three cases [compare Eq. (51) and (52)], the value of $N_1(0)-N_1(\infty)$ will be different. This explains why all three curves do not coincide at $t=0$.

$$\sigma(s)=\sqrt{\frac{D}{s}}\frac{1}{\sinh(\ell\sqrt{s/D})}. \tag{32}$$

The inverse Laplace transforms of $\Delta(s)$, $\kappa(s)$, and $\sigma(s)$ are shown in Eq. (5) and depicted in Fig. 5. The long-time behavior of $\kappa(t)$ and $\sigma(t)$ can be found from a small-s expansion of Eqs. (31) and (32):

$$\kappa(t)\approx\frac{D}{\ell}-\sqrt{\frac{D}{\pi t}},$$

$$\sigma(t)\approx\frac{D}{\ell}\left[1-\exp\left(-\frac{6Dt}{\ell^2}\right)\right]. \tag{33}$$

Taking the limit $t\to\infty$ yields

$$\sigma(\infty)=\frac{D}{\ell},\quad \kappa(\infty)=\frac{D}{\ell}. \tag{34}$$

It is more convenient to express the rate equations (29) in time domains:

$$\dot{N}_1(t)=\frac{V_{d-1}(a)}{V_d(R_2)}\int_0^t dt'\mathcal{N}_2(t')\sigma(t-t')-\frac{V_{d-1}(a)}{V_d(R_1)}\int_0^t dt'\mathcal{N}_1(t')\times[\Delta(t-t')+\kappa(t-t')], \tag{35a}$$

$$\dot{N}_2(t)=\frac{V_{d-1}(a)}{V_d(R_1)}\int_0^t dt'\mathcal{N}_1(t')\sigma(t-t')-\frac{V_{d-1}(a)}{V_d(R_2)}\int_0^t dt'\mathcal{N}_2(t')\times[\Delta(t-t')+\kappa(t-t')]. \tag{35b}$$

$\kappa(t)$ and $\sigma(t)$ are not present in the rate equation for the semi-infinite case [see Eq. (21)] and arise only when the system is finite.

A numerical solution to Eqs. (35) is shown in Fig. 6 (see Appendix A for a more elaborate discussion regarding the numerical procedure). The number of particles decays exponentially which is verified in Fig. 7 where the straight line attained after some time is evidence of a single-exponential decay. The figure also shows a nonexponential regime for small t, described by $\Delta(t)$. Terms proportional to $\Delta(t)$ are in the following referred to as Δ terms.

For small t particles rush into the tube with a large current. At $t=0$ the current is infinite, $\lim_{t\to 0}\dot{N}_1(t)=\infty$. Thus, exactly at $t=0$ it is impossible to define the exit rate from container and such a situation extends to any other time instant. In a *strict* mathematical sense, it is impossible to define exit rate from the container for any $t>0$ (when the concentration profile at the tube opening is different from zero). This can be illustrated with a simple example. Let V be a volume divided into two subvolumes V_1 and V_2 such that V_1 and V_2 touch each other and exchange particles by diffusion. The dynamical variables of interest are the total number of particles in each subvolume, $N_1(t)$ and $N_2(t)$. The goal is to derive some kind of rate equation for $N_1(t)$ and $N_2(t)$. We focus on the flow from V_1 to V_2. In a small time interval ϵ one will have $N_1(t+\epsilon)\propto N_1(t)(1-\alpha\sqrt{\epsilon})$ and $N_2(t+\epsilon)\propto N_2(t)+\beta N_1(t)\sqrt{\epsilon}$, where α and β are numerical constants. The effective exchange rate that describes the flow from V_1 into V_2 is given by

$$k_{21}(t)=\lim_{\epsilon\to 0}\frac{N_2(t+\epsilon)-N_2(t)}{N_1(t)\epsilon}\propto\lim_{\epsilon\to 0}\epsilon^{-1/2}, \tag{36}$$

which is infinite. At any time instant t an infinite amount of particles (per unit time) is rushing from V_1 into V_2 (and vise versa). However, the infinite flows from V_1 to V_2 and the

other way around cancel each other out, resulting in a finite net flow giving smooth curves for $N_1(t)$ and $N_2(t)$. $t=0$ is special since there is no counterflow from V_2 to V_1 which explains why $\lim_{t\to 0}\dot{N}_1(t)=\infty$.

The nonexponential regime grows with tube length ℓ and might play a significant role in studying transport processes in networks having long connections. For large times $\kappa(t)$ and $\sigma(t)$ start to dominate and one observes exponential decay. It will be shown in Sec. V how to derive rate equations that describe this regime.

V. ANALYSIS OF THE GENERAL RATE EQUATION: EMERGENCE OF A SINGLE-EXPONENTIAL SOLUTION

It is intuitively clear that in the case of the two-node network discussed in the previous section one should have an exponential decay (growth) for the number of particles in the container $C_1(C_2)$ (see Figs. 6 and 7): asymptotically the time dependence of $N_1(t)$ and $N_2(t)$ is given by

$$N_{1,2}(t) = N_{1,2}(\infty) + \mathcal{A}_{1,2}\exp(-t/\tau), \tag{37}$$

where τ^{-1} is the decay exponent that governs the late-time asymptotics and $\mathcal{A}_{1,2}$ is the amplitude of decay. This fact is not easily predicted from the form of the general rate equation given in Eq. (3). To understand the emergence of such behavior a more thorough investigation of Eq. (46) is needed.

To obtain the exact value of the decay exponent one has to study the structure of poles of $N_{1,2}(s)$. The poles fully determine the form of $N_{1,2}(t)=\Sigma_{p=0}^{\infty}a_p e^{s_p t}$ where a_p is the residue of $N_{1,2}(s)$ at pole s_p. The values of $N_{1,2}(\infty)$ are determined by the $p=0$ term ($s_0=0$). The exponential decay rate is determined by

$$\tau^{-1} = -s_1. \tag{38}$$

Rewriting Eqs. (29) in matrix form yields

$$s\vec{N}(s) - \vec{N}_0 = \mathcal{M}\vec{N}(s), \tag{39}$$

where

$$\vec{N}(s) = [N_1(s), N_2(s)]^T, \quad \vec{N}_0 = [N_{10}, N_{20}]^T \tag{40}$$

and

$$\mathcal{M} = \frac{qD}{\ell^2}\begin{bmatrix} -\dfrac{V_{\text{tube}}}{V_d(R_1)}\coth q & \dfrac{V_{\text{tube}}}{V_d(R_2)}\dfrac{1}{\sinh q} \\ \dfrac{V_{\text{tube}}}{V_d(R_1)}\dfrac{1}{\sinh q} & -\dfrac{V_{\text{tube}}}{V_d(R_2)}\coth q \end{bmatrix}, \tag{41}$$

with $q^2=s\ell^2/D$ and $V_{\text{tube}}=V_{d-1}(a)\ell$. The poles are calculated from $\det(s-\mathcal{M})=0$ since $\vec{N}(s)=(s-\mathcal{M})^{-1}\vec{N}_0$ and $(s-\mathcal{M})^{-1}\propto 1/\det(s-\mathcal{M})$. Evaluating $\det(s-\mathcal{M})=0$ gives

$$q^2 + q\left[\frac{V_{\text{tube}}}{V_d(R_1)} + \frac{V_{\text{tube}}}{V_d(R_2)}\right]\coth q + \frac{V_{\text{tube}}^2}{V_d(R_1)V_d(R_2)} = 0. \tag{42}$$

Equation (42) is a transcendental equation and has many solutions q_p that determine the value of the poles $s_p=q_p^2 D/\ell^2$ where $p=1,2,\ldots,\infty$ and in particular

$$s_1 = \frac{q_1^2 D}{\ell^2}, \tag{43}$$

which, together with Eq. (38), gives a relationship between q_1 and the decay rate $\tau^{-1}=-q_1^2 D/\ell^2$. Note that q^2 has been factored out from Eq. (42) and $s_0=0$ ($q_0=0$) is the additional pole that determines the values of $N_{1,2}(\infty)$. Also, note that q_1 depends only on parameters describing geometry of the network.

Apart from determining the structure of the poles, Eqs. (39)–(41) are a good starting point for classifying various schemes for obtaining approximative forms of the rate equations given in Eqs. (35). Equations (35) do not have the form of the general rate law stated in Eq. (18) (due to the presence of the Δ terms). Such a rate law would be easier to understand intuitively. For example, the emergence of the single-exponential decay could be seen more easily in Eq. (18) than in Eqs. (35). Also, an approximative form might be easier to implement numerically, though at the cost of a lower accuracy at the end. The idea is to perform a small s expansion of Eq. (39) based on a desired accuracy. In here we consider two cases.

A. Lowest-order expansion

Performing the expansion

$$q\coth q \approx 1, \quad \frac{q}{\sinh q} \approx 1, \tag{44}$$

of $\mathcal{M}$ in Eq. (41) leads to a matrix that is constant, and taking the inverse Laplace transform of Eq. (39) gives the following set of rate equations:

$$\dot{N}_1(t) = -\dot{N}_2(t) = V_{\text{tube}}\frac{D}{\ell^2}\left[\frac{N_2(t)}{V_d(R_2)} - \frac{N_1(t)}{V_d(R_1)}\right]. \tag{45}$$

These equations were already stated in Ref. [9]. It is interesting to see that they emerge as a special case of the scheme discussed here. Also, Eq. (45) can be obtained by following another route. Performing partial integration of Eqs. (35) with terms containing $\Delta(t)$ omitted leads to the exactly the same form of rate equations as given in Eq. (45). This procedure is discussed below.

The Δ terms are only present when the system is infinite. Since the problem is finite, terms proportional to $\Delta(t)$ will be subleading for large t. This can be seen from a small-s (large-t) expansion of Eqs. (23) and (31).[1] Also, partial integration of the Δ terms is impossible since the derivative of $\Delta(t)$ is proportional to $t^{-3/2}$ and diverges when $t\to 0$.

Omitting the Δ terms in Eqs. (35) and performing partial integration leads to

[1] A small-s expansion of Eqs. (23) and (31) in Laplace transform space yields $\mathcal{L}^{-1}[\Delta(s)]\propto t^{-1/2}$ and $\mathcal{L}^{-1}[\kappa(s)]\propto$ const. Since $\Delta(t)$ and $\kappa(t)$ always combine in a sum, $\kappa(t)$ will dominate the outflow for large t.

$$\dot{N}_1(t) = \frac{V_{d-1}(a)}{V_d(R_2)} \int_0^t dt' N_2(t-t')\dot{\sigma}(t') - \frac{V_{d-1}(a)}{V_d(R_1)} \int_0^t dt' N_1(t-t')\dot{\kappa}(t'), \tag{46a}$$

$$\dot{N}_2(t) = \frac{V_{d-1}(a)}{V_d(R_1)} \int_0^t dt' N_1(t-t')\dot{\sigma}(t') - \frac{V_{d-1}(a)}{V_d(R_2)} \int_0^t dt' N_2(t-t')\dot{\kappa}(t'). \tag{46b}$$

Since $\dot{\sigma}(t)$ is peaked for small t (see Fig. 5), the contribution to the integrals (convolutions) stems mainly from small values of t' which justifies the approximation

$$\int_0^t dt' N_{1,2}(t-t')\dot{\sigma}(t') \approx N_{1,2}(t) \int_0^t dt' \dot{\sigma}(t') = N_{1,2}(t)\sigma(t), \tag{47}$$

where $\sigma(0)=0$ was used. The same applies for $\kappa(t)$. Using Eq. (47) in Eq. (46) leads to

$$\dot{N}_1(t) = \frac{V_{d-1}(a)}{V_d(R_2)} N_2(t)\sigma(t) - \frac{V_{d-1}(a)}{V_d(R_1)} N_1(t)\kappa(t), \tag{48a}$$

$$\dot{N}_2(t) = \frac{V_{d-1}(a)}{V_d(R_1)} N_1(t)\sigma(t) - \frac{V_{d-1}(a)}{V_d(R_2)} N_2(t)\kappa(t). \tag{48b}$$

Inserting $\kappa(\infty)$ and $\sigma(\infty)$ found in Eq. (34) into Eq. (48) yields Eq. (45). This example shows how the Δ terms disappear from the description when the system is finite. However, contrary to the partial integration method, the expansion of Eq. (39) gives a more systematic and controlled approach.

Equation (45) is simple and computationally efficient. It could be easily used to describe large networks. However, it has several drawbacks that can be identified. The solution to Eq. (45) is given by

$$N_{1,2}(t) - N_{1,2}(\infty) = [N_{1,2}(0) - N_{1,2}(\infty)]\exp(-t/\tau_{1,a}). \tag{49}$$

The decay rate $\tau_a^{-1} = -q_{1,a}^2 D/\ell^2$ is determined by

$$q_{1,a}^2 = -\frac{V_{\text{tube}}[V_d(R_1) + V_d(R_2)]}{V_d(R_1)V_d(R_2)}. \tag{50}$$

The number of particles in each container as $t \to \infty$ is

$$\frac{N_1(\infty)}{V_d(R_1)} = \frac{N_2(\infty)}{V_d(R_2)} = \frac{N_{10}+N_{20}}{V_d(R_1)+V_d(R_2)}. \tag{51}$$

Equation (51) is not correct. The correct values for $N_{1,2}(\infty)$ are given by

$$\frac{N_1(\infty)}{V_d(R_1)} = \frac{N_2(\infty)}{V_d(R_2)} = \frac{N_{10}+N_{20}}{V_d(R_1)+V_d(R_2)+V_{\text{tube}}}. \tag{52}$$

The discrepancies between Eqs. (51) and (52) become increasingly important for long tubes which are likely to occur in large networks. For example, in a case where the tube and reservoir volumes are equal, Eq. (51) predicts $N_1(\infty) = N_2(\infty) = N_{tot}/2$, $N_{tot} = N_{10} + N_{20}$, while the exact result from Eq. (52) is $N_{tot}/3$. The particle decay exponent given in Eq. (50) only holds when $V_{\text{tube}} \to 0$. It strongly deviates from the exact value when the tube is long (see Fig. 8).

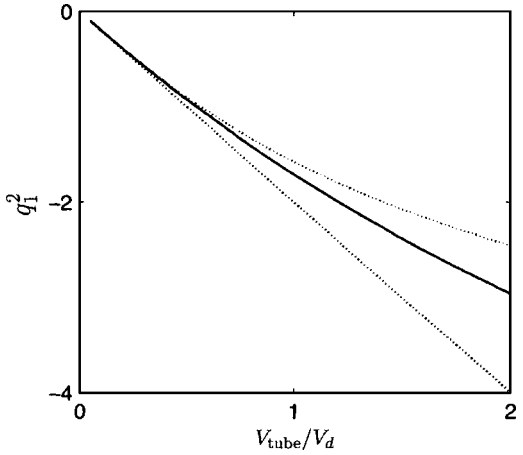

FIG. 8. Dependence of the geometrical factor q_1^2 on the tube volume. [The volumes of the containers are equal, $V_d(R_1) = V_d(R_2) \equiv V_d$.] q_1^2 and τ^{-1} are related through $\tau^{-1} = -q_1^2 D/\ell^2$. The numerical solution of Eq. (42), which gives exact values for q_1^2, is represented by the solid line. It is compared with the values for $q_{1,a}^2$ [Eq. (50)], dashed line, and $q_{1,b}^2$ [Eq. (56)], dotted line. The dotted line deviates significantly from the solid one as V_{tube}/V_d increases while the dashed line follows the exact solution better. This indicates that $q_{1,b}^2$ provides a good estimate of the decay rate, even for large tube volumes. $q_{1,a}^2$ can only be used for very small values of V_{tube}/V_d.

B. Higher-order expansion

Using the expansion

$$q \coth q \approx 1 + \frac{q^2}{3}, \quad \frac{q}{\sinh q} \approx 1 \tag{53}$$

for $\mathcal{M}$, inserting in Eq. (39), and taking inverse Laplace transform leads to a set of rate equations (given in Appendix B) that are unsatisfactory due to the following reasons. First, they predict a spurious jump in $N_{1,2}(t)$ as $t \to 0$ and the limiting values $N_{1,2}(\infty)$ are not correct. Second, the rate exponent that results from these equations is not that accurate. This particular example shows that it is important to have a balanced expansion for elements of $\mathcal{M}$. For example, instead of expanding $q \coth q$ directly one has to expand $\sinh q$ and $\cosh q$ separately in such a way that the same powers in the nominator and denominator are obtained. When this strategy is followed a much better approximation is obtained as shown below.

The next-order expansion gives correct limits for $N_{1,2}(t)$ when $t \to 0$ and $t \to \infty$ and leads to a relatively accurate value for the decay exponent. Using the expansion

$$q \coth q \approx \frac{1 + q^2/2}{1 + q^2/6}, \quad \frac{q}{\sinh q} \approx \frac{1}{1 + q^2/6}, \tag{54}$$

in $\mathcal{M}$ gives the following set of equations:

$$\dot{N}_1(t) = -N_1(t)\frac{3D}{\ell^2}\frac{V_{\text{tube}}}{V_d(R_1)} + \frac{12D^2}{\ell^4}\frac{V_{\text{tube}}}{V_d(R_1)}\int_0^t dt' N_1(t-t') \times\exp\left(-\frac{6Dt'}{\ell^2}\right) - \frac{6D^2}{\ell^4}\frac{V_{\text{tube}}}{V_d(R_2)}\int_0^t dt' N_2(t-t') \times\exp\left(-\frac{6Dt'}{\ell^2}\right), \tag{55a}$$

$$\dot{N}_2(t) = -N_2(t)\frac{3D}{\ell^2}\frac{V_{\text{tube}}}{V_d(R_2)}\frac{12D^2}{\ell^4}\frac{V_{\text{tube}}}{V_d(R_2)}\int_0^t dt' N_2(t-t') \times\exp\left(-\frac{6Dt'}{\ell^2}\right) - \frac{6D^2}{\ell^4}\frac{V_{\text{tube}}}{V_d(R_1)}\int_0^t dt' N_1(t-t') \times\exp\left(-\frac{6Dt'}{\ell^2}\right). \tag{55b}$$

Solving $\det(s-\mathcal{M})=0$ to get hold of the decay exponent in analytical form becomes in this case rather tedious since finding the value q_1 amounts to finding a root of a fourth-degree polynomial. The calculation simplifies somewhat if equal container volumes are considered, $V_d(R_1)=V_d(R_2) \equiv V_d$. In such a case one has

$$q_{1,b}^2 = -\frac{1}{2V_d}[3(2V_d + V_{\text{tube}}) - \sqrt{3(12V_d^2 - 4V_dV_{\text{tube}} + 3V_{\text{tube}}^2)}]. \tag{56}$$

The main findings of this section are summarized in Figs. 6–8. Figures 6 and 7 depict a numerical solution of Eq. (35) (solid line) compared with the approximations discussed in this section for a case where the tube and container volumes are equal. Figure 8 shows a detailed analysis of the decay rate.

For very short times there is a difference between Eqs. (55) and (35) in Figs. 6 and 7. These arise due to the partial elimination of Δ terms. For example, Eq. (55) does not predict $\lim_{t\to 0}\dot{N}_1(t)=\infty$ [Fig. 6, the dashed line lies above the solid line near $t=0$ for curves depicting $N_1(t)$]. This is the reason why the curve for $N_1(t)$ obtained from Eq. (55) underestimates the emptying of container C_1. This effect is more pronounced for the $N_1(t)$ coming from Eq. (49). There, the Δ terms are eliminated altogether [Fig. 6, the dotted line depicting $N_1(t)$ lies above solid and dashed lines]. Also, Fig. 6 shows that there is a large error in $N_{1,2}(\infty)$ for curves obtained by Eqs. (45).

In Fig. 7 the natural logarithm of $[N_1(t)-N_1(\infty)]/N_{tot}$ is shown. For short times the dynamics is not exponential but after some time a straight line is attained which is evidence of single-exponential behavior. The curve corresponding to Eq. (49) (dotted line) does not predict the correct decay exponent which is manifested in a different slope. The decay exponent predicted by Eq. (55) is a better estimate for the decay rate: the slopes of the dashed and solid lines more or less coincide. This fact is shown more clearly in Fig. 8.

Figure 8 depicts the dependence of q_1^2 as a function of the tube volume. The numerical solution to Eq. (42) (solid line), which gives the exact value of the decay exponent, is compared to the values of $q_{1,a}^2$ (dotted line) and $q_{1,b}^2$ (dashed line). All three cases work well when $V_{\text{tube}}\to 0$. As the tube volume increases $q_{1,a}^2$ deviates more and more from q_1^2. The same holds for $q_{1,b}^2$, though its value lies much closer to q_1^2. For example, when all volumes are equal $q_1=-1.71$ and $q_{1,b}^2=-1.63$ while $q_{1,a}^2=-2$.

In this section methods of finding rate equations and decay exponents for the two container problem was deduced. Figures 6–8 show that for increasing tube volumes the rate equations given in Eq. (49) are not capable of describing the dynamics. The approximation given in Eq. (55) works better. For short-time dynamics none of the developed methods are valid and the full rate equation (3) is the only alternative. In the subsequent section all rate equations discussed up to this point will be extended to work for any network structure.

VI. GENERAL EXPRESSION

In this section the results and methods obtained and developed for two-node network will be extended to work for any network structure. The complete dynamics for the two-node network is formulated in Eq. (35). For an arbitrary network the outflow (OUT) from container i to container j is proportional to $\Delta_{ij}(t)+\kappa_{ij}(t)$ and the inflow (IN) from container j to container i is proportional to $\sigma_{ji}(t)$:

$$(\text{OUT})_{i\to j} = \frac{V_{d-1}(a_{ij})}{V_d(R_i)}\int_0^t dt' \mathcal{N}_i(t')[\Delta_{ij}(t-t') + \kappa_{ij}(t-t')], \tag{57a}$$

$$(\text{IN})_{j\to i} = \frac{V_{d-1}(a_{ji})}{V_d(R_j)}\int_0^t dt' \mathcal{N}_j(t')\sigma_{ji}(t-t'). \tag{57b}$$

This implies

$$\dot{N}_i(t) = \sum_{j\neq i}\mathcal{C}_{ij}[(\text{IN})_{j\to i} - (\text{OUT})_{i\to j}], \quad i=1,\ldots,M, \tag{58}$$

where $\mathcal{C}_{ij}$ is the conductivity matrix discussed in Sec. II. The final result is stated in Eq. (3).

It was argued earlier that if the tube volume is small, a very simple first-order rate equation can be stated. It is found in Eq. (45). Extending this equation to the case of arbitrary topology yields

$$\dot{N}_i(t) = \sum_{j\neq i}\mathcal{C}_{ij}V_{d-1}(a_{ij})\frac{D_{ij}}{\ell_{ij}}\left[\frac{N_j(t)}{V_d(R_j)} - \frac{N_i(t)}{V_d(R_i)}\right]. \tag{59}$$

Note the symmetry relations $a_{ij}=a_{ji}$, $\ell_{ij}=\ell_{ji}$, and $D_{ij}=D_{ji}$.

If a more sensitive solution is desired, a set of equations of the type (55) is suggested. An extension of this equation is

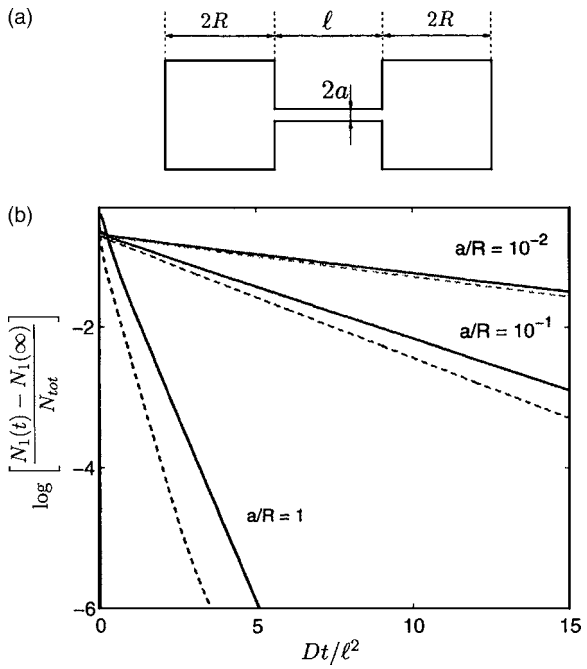

FIG. 9. A numerical verification of the assumption of well-stirred containers. For simplicity reasons a cubic geometry, as depicted in panel (a), was chosen since the explicit shape of the container loses its importance for large reservoir volumes. The edge length is set to $2R$ where R is the radius of an equivalent spheric container. Panel (b) shows a numerical solution to the 2D diffusion equation (solid line) compared to a numerical solution to Eqs. (3) (dashed line). The cases are chosen so that a/R varies in three orders of magnitude, showing increasing validity of the assumption of ideally mixed containers as a/R decreases. The initial distribution in all three cases is skewed (a δ function in the bottom right corner of the left container) which becomes important when a is large. For small a, τ_{mix} is a lot shorter than τ_{target} and the skewed initial distribution will have time to smear out before particles start exiting and the shape of the initial distribution has no effect.

$$(\text{OUT})_{i\to j} = N_i(t)\frac{3D_{ij}}{\ell_{ij}}\frac{V_{d-1}(a_{ij})}{V_d(R_i)} - \frac{12D_{ij}^2}{\ell_{ij}^3}\frac{V_{d-1}(a_{ij})}{V_d(R_i)}\int_0^t dt'\,\exp\left(\frac{-6Dt'}{\ell_{ij}^2}\right)N_i(t-t'), \tag{60a}$$

$$(\text{IN})_{j\to i} = \frac{6D_{ji}^2}{\ell_{ji}^3}\frac{V_{d-1}(a_{ji})}{V_d(R_j)}\int_0^t dt'\,\exp\left(\frac{-6D_{ji}t'}{\ell_{ji}^2}\right)N_j(t-t'). \tag{60b}$$

Inserting Eq. (60) into Eq. (58) yields an approximative form of rate equations for an arbitrary network.

In the previous section we investigated the differences between Eqs. (57), (59), and (60) using the two-node network as a study case ($M=2$). It is expected that the findings of the previous section also apply for larger networks. This analysis is not conducted here. Having general expressions at hand more complicated network structures can be investigated. However, the assumption of well-stirred containers will be discussed first since it is crucial for the derivation of the rate equations (3).

VII. ASSUMPTION OF IDEALLY MIXED CONTAINERS

An ideally mixed container has no concentration gradients. If a particle has entered, it can be found anywhere within the compartment with equal probability. In reality, a diffusing particle examines the compartment in a random walk fashion until an opening is found. There it has a possibility to escape and change the concentration. If the tube radius is small ($a/R \ll 1$), a significantly longer time is required to find an opening and escape than to examine the majority of the compartment. The time needed to examine the majority of the compartment is called mixing time and is given by $\tau_{\text{mix}}=R^2/D$. The time of finding a specific place or target having radius a is given by $\tau_{\text{target}}=(R^2/D)R/a$ [15]. For cubic compartments the radius of the sphere R is replaced by the edge length, in this case $2R$ (see Fig. 9). Thus, we argue that if $a \ll R$, then $\tau_{\text{mix}} \ll \tau_{\text{escape}}$ and the containers can be considered ideally mixed at all times.[2] This is supported by numerics.

Figure 9(b) shows a numerical solution of the diffusion equation in two dimensions in a geometry depicted in Fig. 9(a). The solution clearly shows that the assumption of well-stirred containers becomes very good for $a/R \ll 1$, even for skewed initial distributions. The solution to the diffusion equation was found using a standard implicit finite-difference discretization method [16].

In Fig. 9(b) one observes a systematic discrepancy: the assumption of ideally mixed containers tends to overestimate the decay rate. This derives from the fact that the assumption of well-stirred containers over estimates the number of particles at the tube inlet, leading to a larger exit rate.

VIII. CASE STUDIES

Up to this point the two-node network was the only example discussed. It was used as an elementary building block when constructing the rate equation (3). Such a network is rather simple and does not offer any spectacular behavior. In this section more complicated structures will be studied, which are shown in Fig. 10 (and Fig. 17, below): Two realizations of a three-node network are studied first, cases 1 and 2, depicted in Figs. 10(a) and 10(b). They possess one more level of complexity than the two-node network shown in Fig. 4. Case 3, Fig. 10(c), is a four-node network that has a T-shape structure. Case 4, Fig. 10(d), has the shape of a star and involves a tube junction. It will be shown that the transport properties of this structure can be controlled in such way that it might serve as a diffusion-based transistor. These three- and four-node networks, despite being rather simple,

[2] τ_{target} is derived under the assumption of a fully absorbing target of radius a. This is not a correct description of a tube opening since it allows reentry. This estimate serves, however, as a worst-case scenario.

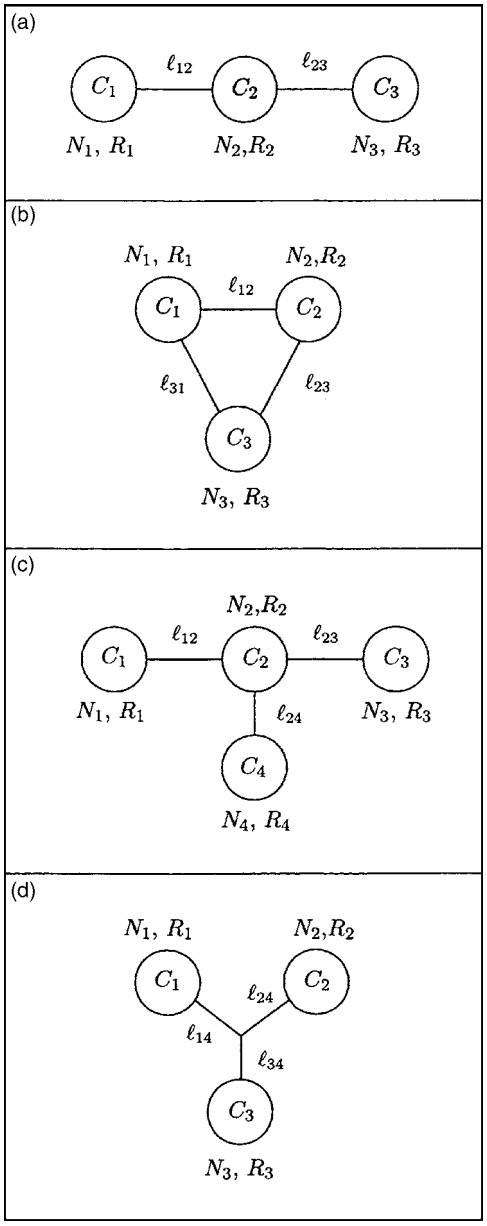

FIG. 10. Networks used for case studies in Sec. VIII. Panels (a)–(d) correspond to cases 1–4.

exhibit a large variety of outputs. Case 5 (Fig. 17, below) demonstrates the transport properties for larger networks that are impossible to predict without using Eq. (3). When solving Eq. (3) numerically the containers and tubes are considered three dimensional. Moreover, the diffusion coefficients D_{ij} and the tube radii a_{ij} were kept the same for all tubes. All graphs are scaled with the total number of particles in the system, $N_{tot}=\Sigma_{i=1}^{M}N_i(0)$.

Case 1: the line. Three reservoirs are lined up on a straight line as depicted in Fig. 10(a). The transport equations for this system can easily be written down using Eq. (3) and are listed in Appendix C 1. A numerical solution is shown in Fig. 11. This three-node system exhibits a new characteristic that cannot be found in the two-node network. The curve depicting the number of particles in the middle container (solid line) has a maximum (an extremum) point.

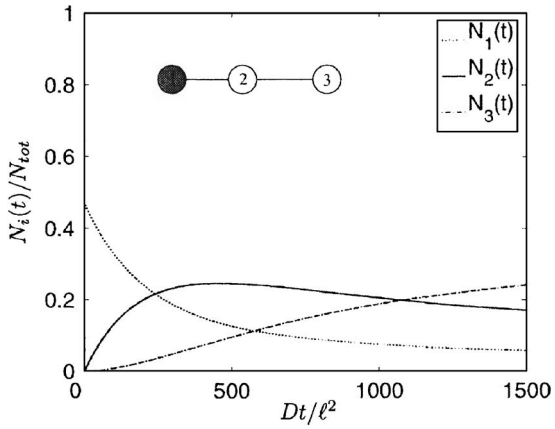

FIG. 11. The transport properties of the structure depicted in Fig. 10(a) [see Sec. VIII (case 1) for a discussion]. The curves depict a numerical solution of Eqs. (C1) and (C2) given in Appendix C 1. The curve depicting the number of particles in the middle container C_2 (solid line) has a maximum. This kind of behavior does not exist for the two-node network where there is only exponential growth and decay (see Fig. 6). The network parameters were set to $\ell_{12}=\ell_{23}\equiv\ell$, $a/\ell=1/5$, $a/R_1=1/10$, $a/R_1=1/15$, and $a/R_3=1/20$. The initial distribution of particles is $N_1(0)/N_{tot}=1$ and $N_2(0)/N_{tot}=N_3(0)/N_{tot}=0$, shown graphically in inset.

The extremum point is a manifestation of an unbalance between inflow and outflow in the middle container. This unbalance derives from an asymmetry in the structure and arises only when $\ell_{12}<\ell_{23}$ or $V_1<V_3$. This provides the possibility of designing the output pattern through simple geometrical changes in the structure. Figure 12 is a simple demonstration of this design possibility where ℓ_{12} is varied so that the arrival time of the maximum of $N_2(t)$, depicting the number of particles in the middle compartment C_2, is changed. The picture also shows that an increase in ℓ_{12} results in both an increased arrival time and a wider peak. The height of the maximum is controlled by the value V_2. A decrease in V_2 suppresses the peak and vice versa.

Case 2: the triangle. The connectivity of the line is

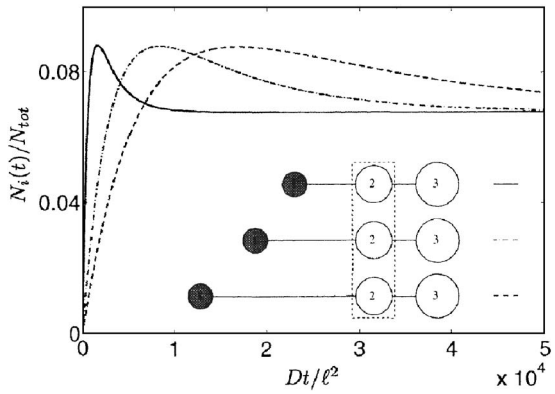

FIG. 12. The control of the particle arrival time for three different cases shown in the inset: $\ell=\ell_1$ (solid line), $\ell/\ell_2=1/5$ (dash-dotted line), and $\ell/\ell_3=1/10$ (dashed line). The system is otherwise equivalent to the one studied in Fig. 11. The initial distribution of particles is shown graphically in the inset.

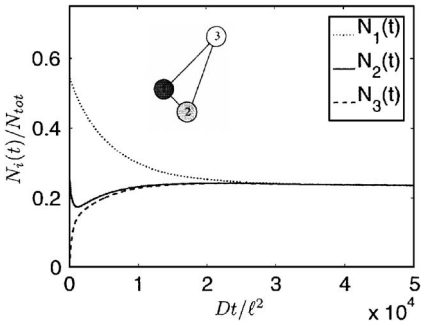

FIG. 13. The transport properties for the triangular network shown in Fig. 10(b) [see Sec. VIII (case 2) for a discussion]. The curves depict a numerical solution of Eq. (C4) given in Appendix C 2. The curve depicting the number of particles in C_2 (solid line) has a minimum. This does not occur in the transport dynamics for the two-node network where there is only exponential growth and decay (see Fig. 6). The parameters were set to $\ell \equiv \ell_{21}$, $\ell/a=1$, $\ell_{23}/\ell=1/10$, $\ell_{31}/\ell=50$, and $R_1/\ell=R_2/\ell=R_3/\ell=4$. The initial distribution of particles is $N_1(0)/N_{tot}=1$, $N_2(0)/N_{tot}=0.5$, and $N_3(0)/N_{tot}=0$ as indicated by shading in the inset.

changed by adding an extra link between containers C_1 and C_3 so that it forms the shape of a triangle, as shown in Fig. 10(b). The rate equations are derived in Appendix C 2, and a numerical solution is shown in Fig. 13. The initial distribution of particles (see the inset in Fig. 13) is chosen in such a way that a minimum is produced in the curve depicting the number of particles in container C_2.

The extremum point can be enhanced or removed completely in the same way as was demonstrated for case 1. Such a minimum will be absent unless the geometry and initial distribution of particles are tailored in a specific way. In general, such a sensitivity of geometrical changes and changes in the location where particles are injected is observed for all cases studied in this section.

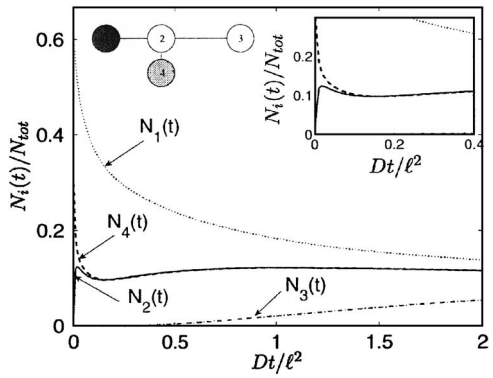

FIG. 14. The transport properties for the T-shaped network shown in Fig. 10(c), [see Sec. VIII (case 3) for a discussion]. The curves depict a numerical solution of Eqs. (C6) and (C7) given in Appendix C 2. The figure shows two extremum points in the curve depicting the number of particles in container C_2 (solid line). It is not possible to have this kind of behavior for any of the cases studied involving two and three containers. The additional extremum point was produced by adding an additional container C_4 to the middle container C_2 in the linear structure shown in Fig. 10(a). The network parameters used were $\ell_{12} \equiv \ell$, $\ell/a=3$, $\ell/\ell_{23}=1/2$, $\ell/\ell_{24}=10$, and $R_1/\ell=2$. The initial distribution was set to $N_1(0)/N_{tot}=2/3$, $N_2(0)/N_{tot}=0$, $N_3(0)/N_{tot}=0$, and $N_4(0)/N_{tot}=1/3$ according to shading in the inset.

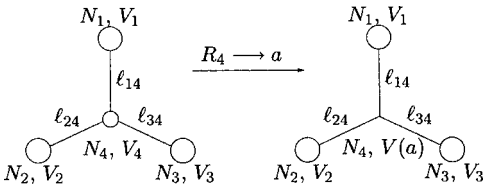

FIG. 15. The transformation from a four-node network to a network involving a three-way junction.

Case 3: the T-shape network. It is interesting to see how the behavior of cases 1 and 2 changes when a new node is added to the network. Here we study a situation where an extra node C_4 is connected to container C_2 in the structure depicted in Fig. 10(a). In such a way one gets a T-shaped (star) network shown in Fig. 10(c). This alternation of structure leads to a significant change in behavior, as shown in Fig. 14. When compared to cases 1 (one maximum) and 2 (one minimum) the curve depicting $N_2(t)$ exhibits an additional extremum point: both minimum and maximum are present simultaneously. The right inset in Fig. 14 emphasizes this fact.

This scheme could be carried out further, adding on more and more reservoirs and adjusting the lengths and the initial distribution so that the peaks arrive in consecutive order, possibly produce an wavelike behavior. However, since the spread of the peaks increases with increasing tube length, it might be numerically quite difficult to see when the the extremum points occur or even if they actually exist.

Case 4: the junction. The next interesting network to consider is the one with a junction present as depicted in Fig.

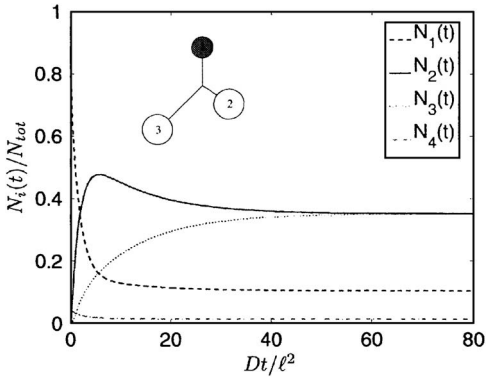

FIG. 16. The transport properties for the network involving a three-way junction shown in Fig. 10(d) [see Sec. VIII (case 4) for a discussion]. The curves depict a numerical solution of Eqs. (C6) and (C7) [with $V_d(R_4)=V_d(a)$]. The system parameters were set to $\ell_{12}/a=2$, $\ell_{13}/a=10$, $\ell_{14}/a=20$, $R_1/a=2$, and $R_2/a=R_3/a=4$. Initial distribution of particles, $N_1(0)/N_{tot}=1$ and $N_2(0)/N_{tot}=N_3(0)/N_{tot}=N_4(0)/N_{tot}=0$, is shown in the inset.

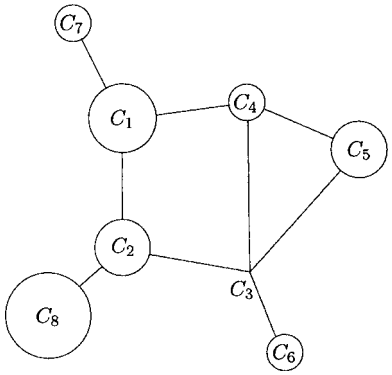

FIG. 17. Structure of the network studied in Sec. VIII (case 5). The parameters describing the geometry are labeled in the same way as in Fig. 10. The parameters used were $a/\ell=1/3$, $\ell_{23}/\ell=1$, $\ell_{45}/\ell=9$, $\ell_{43}/\ell=10$, $\ell_{35}/\ell=8$, $\ell_{36}/\ell=2$, $\ell_{28}/\ell=0.1$, $\ell_{12}/\ell=1$, $\ell_{32}/\ell=1$, $R_1/a=4$, $R_2/a=2$, $R_3/a=1$, $R_4/a=2.5$, $R_5/a=3$, $R_6/a=2$, $R_7/a=2$, and $R_8/a=4$.

10(d). A particular example of a three-way junction is studied. The network is built up by three reservoirs and three tubes. The ends of the tubes coincide to form a junction. To obtain the transport properties of such a network we start from the structure studied in case 3 shown in Fig. 10(c). The junction is obtained by reducing the radius of container C_2 in the middle until its radius is roughly equal to the radii of the surrounding tubes (see Fig. 15). The rate equations describing the junction properties have the same form as the equations describing case 3 (listed in the Appendix C 3) with the substitution $V_d(R_3)\rightarrow V_d(a)$. The equations are not given in order to save space.

A numerical solution of the rate equations for the junction is shown in Fig. 16. This structure allows control of the particle flow between V_1 and V_3 by adjusting the volume V_2 and length ℓ_{24} (see Fig. 15). This setup could function as a diffusion-based transistor. For example, by making ℓ_{24} shorter than ℓ_{34}, compartment C_2 will initially attract diffusing particles from C_1 to a greater extent than C_3, causing a time delay in the particle arrival into container C_3.

This fact is illustrated in Fig. 16 where the maximum in the curve for the number of particles in container C_2 (solid line) indicates an initial accumulation of particles in C_2: $N_2(t)/N_{tot}$ rises from 0 to 0.5 in the interval $t=0$ to $Dt/\ell^2=5$. In this interval container C_2 accumulates the majority of the particles released from container C_1. After the peak has been reached the particles accumulated in C_2 are released into C_3: $N_2(t)/N_{tot}$ continuously drops from value of 0.5 after $Dt/\ell^2=5$. By changing ℓ_{24} the curve for $N_2(t)$ can be manipulated exactly in the same way as done in Fig. 12, but such an analysis is not repeated.

For large networks involving junctions it might be desirable to decrease the number of equations required to solve the transport problem. It is demonstrated in Appendix D that the presence of junctions can be eliminated altogether when investigating dynamics in the $t\rightarrow\infty$ regime for structures having large container volumes ($a\ll R_i$, $i=1,\ldots,M$). Equations (D8)–(D10) show this explicitly for the three-node junction studied here.

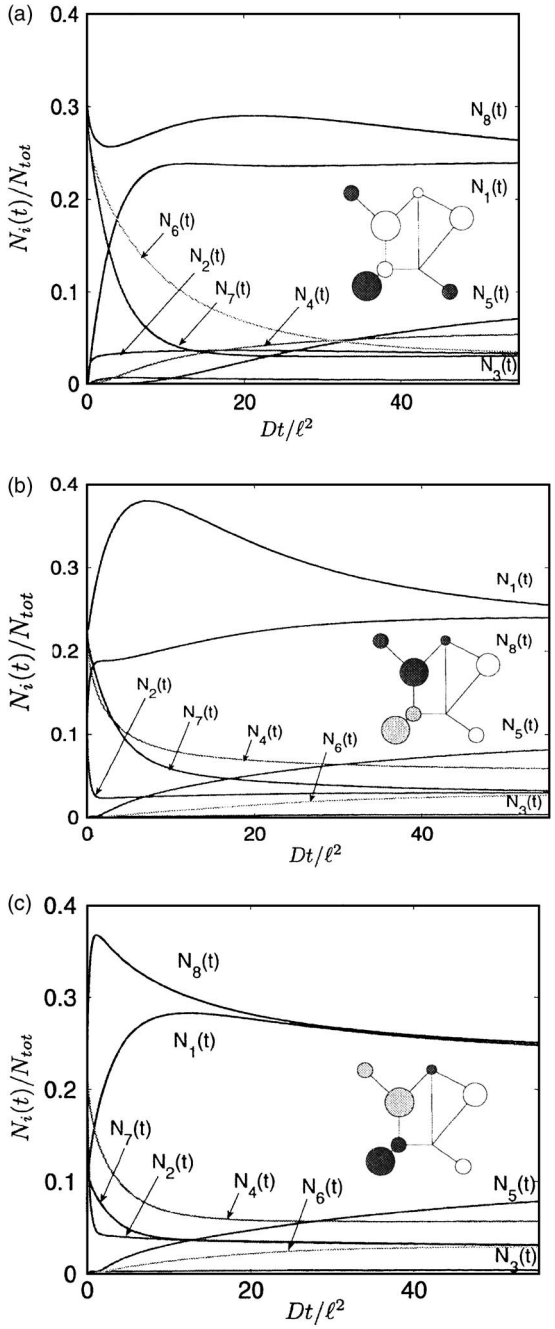

FIG. 18. The solution of Eq. (3) for the network depicted in Fig. 17. The panel includes graphs showing the transport dynamics for three different choices of initial distribution of particles. (a) $\tilde{N}_1(0)=\tilde{N}_2(0)=\tilde{N}_3(0)=\tilde{N}_4(0)=\tilde{N}_5(0)=0$, and $\tilde{N}_6(0)=\tilde{N}_7(0)=\tilde{N}_8(0)=1/3$. (b) $\tilde{N}_3(0)=\tilde{N}_5(0)=\tilde{N}_6(0)=0$, $\tilde{N}_2(0)=\tilde{N}_8(0)=1/8$, and $\tilde{N}_1(0)=\tilde{N}_4(0)=\tilde{N}_7(0)=1/4$; (c) $\tilde{N}_3(0)=\tilde{N}_5(0)=\tilde{N}_6(0)=0$, $\tilde{N}_1(0)=\tilde{N}_7(0)=1/8$, and $\tilde{N}_2(0)=\tilde{N}_4(0)=\tilde{N}_8(0)=1/4$, where $\tilde{N}_i(t)=N_i(t)/N_{tot}$, $i=1,\ldots,8$. The initial conditions are also illustrated in the insets: a darker shading indicates that more particles are injected into the container.

The four cases studied up to now show that the transport dynamics is very sensitive to geometrical changes and to the locations where particles are injected. Small variations in tube lengths and container volumes lead to unpredictable

changes in curves depicting the time dependence of the number of particles in each container (Figs. 11, 13, 14, and 16). Also, the shapes of the curves differs significantly from a single exponential decay.

Case 5: large network. Following the methods described in this paper one could easily study diffusive transport in networks containing hundreds or thousands of containers, tubes, and junctions. The computational cost scales linearly with both the number of containers and number of tubes (assuming full connectivity of the containers). We do not show explicit example with such large number of containers. To demonstrate the power of the method we study a more pedagogical example, the case of a network that is built up by seven containers, nine tubes, and a four-way junction. In contrast to the previous cases shown in Fig. 10 it is impossible to predict the transport behavior of such a network without a numerical calculation.

For the network depicted in Fig. 17, Figs. 18(a)–18(c) show numerical solutions of Eq. (3). Different initial distributions are used and are introduced into the inset of all figures. The darker the container appears, the more particles are injected into it. The dynamics is evidently quite complex, and all possible characteristics that were forced upon the other cases are present. There is an exponential growth and decay as well as curves having one or more extremum points. The different transport behavior shown in Fig. 18 stem only from different initial conditions. If the structure no longer remained fixed, even more complicated patterns could be produced; only imagination sets the limits.

IX. CONCLUDING REMARKS

We introduced a generic model for diffusive particle transport in large networks made of containers and tubes. The diffusion equation that describes the distribution of particles, $\rho(\vec{r},t)$, throughout the network was taken as a starting point. Instead of calculating $\rho(\vec{r},t)$ explicitly, we followed another route and developed a theoretical technique to solve the transport problem using a finite number of variables $N_1(t),\ldots,N_M(t)$ that describe the number of particles in each container. First, a set of rate equations was derived for the two-node network and, second, they were generalized to work for an arbitrary network structure. In such a way we obtained the rate equations that govern the dynamics of $N_1(t),\ldots,N_M(t)$. These equations are summarized in Eq. (3) and are the central result of the paper.

The transport equations were found by study the exchange of chemicals between the container and tube. It was demonstrated in Sec. III how to couple the dynamics in the containers and tubes, as stated in Eqs. (6) and (8)–(10). However, the coupling is too complicated to be carried out in practice in the original form. Several approximations were made in order to make such a scheme doable.

The tubes were assumed to be one-dimensional lines [see Eq. (8)], and the transport in the tubes was described in terms of a one-dimensional diffusion problem involving the concentration profile along the line $c(x,t)$. The expression for $c(x,t)$ can be found analytically using, e.g., the Laplace transform technique. In such a way the tubes were eliminated from the problem.

We have considered diffusive noninteracting point particles, which is a plausible assumption for dilute solutions. One could consider the situation when the particles disturb each other. In that respect, the region of the tube interior is the most critical since the tubes can be very narrow and exclusion effects will be mostly pronounced in there. Such effects could be added into the theoretical description by using results obtained from studies on diffusion with exclusion in one-dimensional systems [17–19]. We expect a very different transport behavior when the diameters of the tubes become comparable in size to those of the particles.

The dynamics in the container is not tractable analytically but it was argued that when the tube radii are smaller than any other length scales in the system (e.g., tube lengths or container radii) the containers can be treated as ideally mixed at all times. This assumption was verified numerically in Sec. VII and simplifies all intracontainer dynamics to one dynamical variable: the total number of particles in a given compartment.

Evidently much of the container dynamics has been neglected but the coupling is formulated in such a way that a more detailed description can be developed should there be a need for that. For example, the container dynamics could be better treated by using the techniques presented in, e.g., [9] or by further exploration of the coupling equations (6) and (8)–(10). For example, one could keep the second term on the right-hand side of Eq. (12) and use $\rho(0,y,z,t)=N(t)/V_d(R)-J(t)/4D_c a$ instead of $\rho(0,y,z,t)=N(t)/V_d(R)$. This procedure would lead to similar rate equations as presented here with different forms for $\Delta(t)$, $\kappa(t)$, and $\sigma(t)$.

Initially the particles feel as if they are escaping from the container into an infinitely long tube. In this regime the number of particles in the container decays nonexponentially. We have identified terms in the rate equations describing this behavior: all terms in Eq. (3) proportional to $\Delta(t)$ dominate when time is small. This nonexponential regime grows with increasing tube length, and the crossover time for this regime scales as ℓ^2/D. Also, terms containing $\Delta(t)$ contain solely a dependence on $\dot{N}_i(t)$ and cannot be rewritten in a form that would involve $N_i(t)$. Accordingly, it is impossible to rewrite Eq. (3) so that it adopts the form of a general rate law [see Eq. (18)]. These issues were discussed in Sec. III. The bottleneck lies in the definition of the transport rate which, in principle, is an ill-defined quantity (see the discussions at the end of Secs. III and IV).

Eventually, for large times the decay is exponential. In such a regime the term proportional to $\Delta(t)$ can be neglected in the rate equation (3). Other terms proportional to $\kappa(t)$ and $\sigma(t)$ can be rewritten in the form of a general rate law, leading to Eqs. (59) and (60). We showed that Eq. (59) is a special case of the general approximation scheme developed in Sec. V: starting from rate Eq. (3) in Laplace transform space we developed a series of approximations that can be used to systematically describe the asymptotic regime, resulting in Eq. (60). Also, we have developed a procedure that can be used to eliminate junction points for large times which reduces the number of variables further (see Appendix D).

Already simple case studies that were used to illustrate the workings of the method exhibit interesting behavior. For example, one can identify three types of curves that appear in the plots depicting the time dependence of the particle number in each container (Figs. 11–14 and 16). Type-I curves occur for the two-node network. These lack extremum points, and the particle number either strictly rises or drops to saturate to asymptotic values. Type-II curves have one maximum or minimum, and type-III curves can have more and these are the most interesting. Type-II and -III curves normally describe the particle number for the container in the network interior.

The existence of type-I curves for large networks suggests that it could be possible to understand the transport between two nodes in terms of an effective two-node network where a complicated structure of links and containers in between two nodes is mapped onto an effective link connecting them. One can raise a more general question: what is the smallest network that would have the same transport properties as some substructure of a given large network? For example, if one is interested in only three nodes of the structure depicted in Fig. 17—e.g., C_5, C_7, and C_8—is there a star-type network—e.g., such as the one depicted in Fig. 10(c) or 10(d)—that would have equivalent transport properties?

The presence of type-II and -III curves indicates the possibility that there might be curves that possess a larger number of extremum points. These are likely to occur in larger networks. We can of course manually enhance certain properties such as the height and width of peaks. This will, however, become more and more complicated as the network size increases. The problem is that the peaks that occur later have a larger width and might be harder to see. For design purposes, it is therefore necessary to build a learning mechanism or a search engine, on top of our existing software, to select certain characteristics in the curves depicting the time evolution of $N_1, \ldots, N_M$. Furthermore, to exploit such effects one has to amplify them in some way. At the moment our study deals with transport only, but reactions in the containers can be included as well, and they could be tailored to amplify such effects (e.g., by choosing a reaction of enzymatic type).

The techniques developed in this work can be used to study transport in various systems. In the following we give a few examples.

(i) Although we exclusively study transport, our model can serve as a platform for reaction-diffusion-based biocomputing devices [4–6,20–34]. In particular, our work is applicable to studies of the reaction-diffusion neuron [28–34]. The reaction-diffusion neuron is an two-dimensional array of compartments that exchange chemicals by diffusion.

(ii) A large number of processes happening in the cell are governed by transport of reactants and chemical reactions. In order to avoid a need for excessive storage facilities the chemical compounds are routed in an orderly fashion between various places within and between the cells and the chemical components arrive exactly at the right place at the right time [15,35]. The setup in Fig. 1 captures this aspect of the cell interior.

(iii) The transport on abstract mathematical networks (nodes and links) has been studied extensively [36,37]. Such studies are geometry free with emphasis on the topology of the network graph (the connectivity pattern, the average number of neighbors, etc.). The techniques developed in this work could be used to account for the fact that the links between the nodes have physical length and the transport along the links is not instantaneous.

In summary, the work we have presented is a step towards understanding the transport properties of large networks where geometrical concepts such as the length of the tubes play an important role. The setup employed in this study is rather simple. In order to be able to focus on issues related to transport, the reactions are totally omitted. The concentration profile in containers is assumed flat, and this is good approximation when the tubes are thin. Already simple examples of the networks we studied show a number of interesting properties. For example, the transport properties of the networks exhibit a large sensitivity to geometrical changes in the structure. Also, one can adjust the structure to obtain wavelike behavior (with one or two extremum points) in the curves that depict the number of particles in containers. When the complexity of the network increases one can expect even more complicated behavior with a larger number of extremum points. The setup we use is generic, and it is possible to expand the model in many ways—e.g., by improving description of intracontainer dynamics, incorporating reactions, or allowing particles to disturb each other. It will be an interesting problem to try to explore these questions further.

ACKNOWLEDGMENTS

We would like to thank Professor Owe Orwar and Professor Mats Jonson for fruitful discussions. The financial support of Professor Owe Orwar is greatly acknowledged.

APPENDIX A: NUMERICAL CONSIDERATIONS

In this section the numerical solution of Eq. (3) is discussed. In Secs. III and IV it was shown that the time derivatives $\dot{N}_i(t), \ldots, \dot{N}_M(t)$ can be infinite at $t=0$ which may cause numerical difficulties. However, the singular part of the derivative can be factored out by making the substitution

$$\dot{N}_i(t) = -(\pi t)^{-1/2}\psi_i(t), \quad i = 1, \ldots, M, \tag{A1}$$

where $\psi_i(t)$ is a smooth function of time. For small t the particles in the containers do not (yet) "feel" the presence of another side and behave as if entering an infinitely long tube. An expression describing the transport behavior for such a case was found analytically and is stated in Eq. (20). The time derivative of Eq. (20) is proportional to $t^{-1/2}$ for small t. Inserting Eq. (A1) into Eq. (3) yields an equation for $\psi_i(t)$ that was used for numerical calculations:

$$\psi_i(t) = \sum_{j=1}^{M} \mathcal{C}_{ji} \frac{V_{d-1}(a_{ji})}{V_d(R_j)} \left[\sqrt{\frac{t}{\pi}} \int_0^t \frac{dt'}{\sqrt{t'}} \psi_j(t') \sigma_{ji}(t-t') + \sqrt{\pi t} N_j(0) \sigma_{ji}(t) \right] - \sum_{j=1}^{M} \mathcal{C}_{ij} \frac{V_{d-1}(a_{ij})}{V_d(R_i)} \times \left[\sqrt{\frac{t}{\pi}} \int_0^t \frac{dt'}{\sqrt{t'}} \psi_i(t') \kappa_{ij}(t-t') + \frac{\sqrt{D_{ij} t}}{\pi} \right.$$

$$\times \int_0^t \frac{dt'}{\sqrt{\{t(t-t')\}}} \psi_i(t') + \sqrt{\pi t} N_i(0)[\Delta_{ij}(t) + \kappa_{ij}(t)] \Bigg]. \tag{A2}$$

Note that the expression for $\Delta_{ij}(t)$ has been inserted into the integrals. Combining Eq. (20) and (A1) leads to

$$\psi_i(t) = N_{i0} - (\pi t)^{1/2} N_i(t), \quad i = 1, \ldots, M, \tag{A3}$$

and sets the initial condition $\psi_i(0) = N_{i0}$.

From Eq. (A2) two types of integrals can be identified:

$$I_1^{t_n}[\psi] = \int_0^{t_n} \frac{dt'}{\sqrt{t'(t_n - t')}} \psi(t'),$$

$$I_2^{t_n}[\psi] = \int_0^{t_n} \frac{dt'}{\sqrt{t'}} \psi(t'), \tag{A4}$$

where $\psi(t)$ is nonsingular in the range of integration. The quadrature formulas derived to solve $I_1^{t_n}[\psi]$ and $I_2^{t_n}[\psi]$ are based on the methods described in [38]. The idea is that the singular part of the integrand, $t'^{-1/2}$ and $[t'(t_n - t')]^{-1/2}$, respectively, is treated exactly while the smooth part $\psi_i(t')$ is linearly interpolated between t_i and t_{i+1}. The resulting quadrature formulas are of the form

$$I_i^{t_n}[\psi] \approx \sum_{j=0}^{n} w_{nj} \psi(t_j), \quad i = 1,2, \tag{A5}$$

where w_{nj} are weights, $n = 1, 2\ldots$, and $t_n = nh$. This quadrature formula becomes exact when $\psi(t)$ is piecewise linear. Calculating weights for $I_1^n[\psi]$ yields

$$w_{n0} = \sqrt{n-1} - (n-2)\arcsin\sqrt{\frac{1}{n}},$$

$$w_{ij} = \sqrt{(j-1)(n-j+1)} + \sqrt{(j+1)(n-j-1)} - 2\sqrt{j(n-j)} + 2\left(j + 1 - \frac{n}{2}\right)\left[\arcsin\sqrt{\frac{j-1}{n}} - 2\arcsin\sqrt{\frac{j}{n}} + \arcsin\sqrt{\frac{j+1}{n}}\right],$$

$$w_{nn} = \sqrt{n-1} + \pi\left(1 - \frac{n}{2}\right) + (n-2)\arctan\sqrt{n-1}. \tag{A6}$$

Calculating weights for $I_2^n[\psi]$ yields

$$w_{n0} = \frac{4h^{1/2}}{3},$$

$$w_{nj} = \frac{4h^{1/2}}{3}[(j+1)^{3/2} - 2j^{3/2} + (j-1)^{3/2}],$$

$$w_{nn} = \frac{2h^{1/2}}{3}[n^{3/2} - 3(n-1)^{1/2} + 2(n-1)^{3/2}]. \tag{A7}$$

Finally, an expression for the total number of particles is found by integrating Eq. (A1):

$$N_i(t) = N_i(0) - \int_0^t \frac{dt'}{\sqrt{t'}} \psi_i(t'), \quad i = 1, \ldots, M. \tag{A8}$$

$N_i(t), \ldots, N_M(t)$ are found by using the quadrature formula derived for $I_2^n[\psi]$.

APPENDIX B: FINDING A SET OF APPROXIMATIVE RATE EQUATIONS FROM AN EXPANSION OF Eq. (39) IN THE VARIABLE *s*

In this appendix, details for obtaining a set of a first-order rate equations from Eq. (39) will be outlined. The dynamical equations are found by approximating $\mathcal{M}$ given in Eq. (41). $\mathcal{M}$ is approximated by using the expansion stated in Eq. (53). The inverse Laplace transform of Eq. (39) after approximation reads

$$\dot{N}_1(t) = \frac{3V_d(R_1)V_{\text{tube}}}{3V_d(R_1) + V_{\text{tube}}} \frac{D}{\ell^2}\left[\frac{N_2(t)}{V_d(R_2)} - \frac{N_1(t)}{V_d(R_1)}\right] - \delta(t)\frac{V_{\text{tube}}}{3V_d(R_1) + V_{\text{tube}}} N_{10}, \tag{B1a}$$

$$\dot{N}_2(t) = \frac{3V_d(R_2)V_{\text{tube}}}{3V_d(R_2) + V_{\text{tube}}} \frac{D}{\ell^2}\left[\frac{N_1(t)}{V_d(R_1)} - \frac{N_2(t)}{V_d(R_2)}\right] - \delta(t)\frac{V_{\text{tube}}}{3V_d(R_2) + V_{\text{tube}}} N_{20}. \tag{B1b}$$

The decay rate predicted by these equations is given by $\tau_{1,b'}^{-1} = -\ell^2 / q_{1,b'}^2 D$ where

$$q_{1,b'}^2 = -\frac{V_{\text{tube}}[V_d(R_1) + V_d(R_2)]}{V_d(R_2)[V_d(R_1) + V_{\text{tube}}/3]}. \tag{B2}$$

This decay exponent is not adequate. For example, in the case where all volumes are equal $q_{1,b'}^2 = -1.5$ while the exact value is $q_{\text{exact}} = -1.71$.

The rate equation (B1) cannot describe the behavior of $N_{1,2}(t)$ as $t \to \infty$ and $t \to 0$: the values for $N_{1,2}(\infty)$ are given by

$$\frac{N_1(\infty)}{V_d(R_1)} = \frac{N_2(\infty)}{V_d(R_1)} = \frac{N_{10} + N_{20}}{V_d(R_1) + V_d(R_2) + \frac{2}{3}V_{\text{tube}}} \tag{B3}$$

and for $N_{1,2}(0^+)$ there is a sudden jump,

$$N_i(0^+) = \frac{N_{i0}}{1 + V_{\text{tube}}/3V_d(R_i)}, \quad i = 1,2, \tag{B4}$$

and $N_i(0^+) \neq N_i(0)$. This is not satisfactory, and another type of expansion is needed if correct limits and better decay rates are to be found.

APPENDIX C: RATE EQUATIONS FOR THE CASE STUDIES

This appendix explains in more detail how to derive the rate equations used in the cases studies in Sec. VIII. The

equations are obtained from Eq. (3). Also, Eq. (59) is used to illustrate the impact on dynamics from changes in the network structure in a less complicated form. The $\mathcal{N}_i(t)$, $\Delta_{ij}(t)$, $\kappa_{ij}(t)$, and $\sigma_{ij}(t)$ are defined in Sec. II. The initial distribution is set to be $N_j(0)=N_{j0}$ where $j=1,\ldots,M$ and M is the total number of nodes in the system. Note the symmetry relations $a_{ij}=a_{ji}$, $\ell_{ij}=\ell_{ji}$, and $D_{ij}=D_{ji}$, which imply that $\kappa_{ij}(t)=\kappa_{ji}(t)$, $\Delta_{ij}(t)=\Delta_{ji}(t)$, and $\sigma_{ij}(t)=\sigma_{ji}(t)$ [see Eq. (5)].

1. Line

The structure of the linear network studied here is shown in Fig. 10(a). Containers C_1 and C_3 are connected only to the middle container C_2. Therefore, the rate equations describing the dynamics in each container, $N_1(t)$ and $N_3(t)$, respectively, have a similar form

$$\dot{N}_i(t) = \frac{V_{d-1}(a_{2i})}{V_d(R_2)}\int_0^t dt'\mathcal{N}_2(t')\sigma_{2i}(t-t') - \frac{V_{d-1}(a_{i2})}{V_d(R_i)}\int_0^t dt'\mathcal{N}_i(t')[\kappa_{i2}(t-t')+\Delta_{i2}(t-t')], \quad i=1,3. \tag{C1}$$

The middle container C_2 is connected both to container C_1 and C_3. The rate equation for $N_2(t)$ reads

$$\dot{N}_2(t) = \frac{V_{d-1}(a_{12})}{V_d(R_1)}\int_0^t dt'\mathcal{N}_1(t')\sigma_{12}(t-t') + \frac{V_{d-1}(a_{32})}{V_d(R_3)}\int_0^t dt'\mathcal{N}_3(t')\sigma_{32}(t-t') - \frac{V_{d-1}(a_{21})}{V_d(R_2)}\int_0^t dt'\mathcal{N}_2(t')[\kappa_{21}(t-t')+\Delta_{21}(t-t')] - \frac{V_{d-1}(a_{23})}{V_d(R_2)}\int_0^t dt'\mathcal{N}_2(t')[\kappa_{23}(t-t')+\Delta_{23}(t-t')]. \tag{C2}$$

Equations (C1) and (C2) have a quite complicated structure and impacts on the dynamics of $N_1(t)$, $N_2(t)$, and $N_3(t)$ due to the fact that changes in the structure (e.g., tube lengths and container volumes) are not easily predicted. Simpler expressions can be obtained by using Eq. (59) which is valid in the large-time limit under the assumption that the number of particles in the tubes is negligible over time. Applying Eq. (59) leads to

$$\dot{N}_i(t) = \frac{V_{d-1}(a_{2i})}{V_d(R_2)}\frac{D}{\ell_{2i}}N_2(t) - \frac{V_{d-1}(a_{i2})}{V_d(R_i)}\frac{D}{\ell_{i2}}N_i(t), \quad i=1,3,$$

$$\dot{N}_2(t) = \frac{V_{d-1}(a_{12})}{V_d(R_2)}\frac{D}{\ell_{12}}N_1(t) + \frac{V_{d-1}(a_{32})}{V_d(R_3)}\frac{D}{\ell_{32}}N_3(t) - \frac{D}{V_d(R_2)}\left[\frac{V_{d-1}(a_{12})}{\ell_{12}}+\frac{V_{d-1}(a_{23})}{\ell_{23}}\right]N_2(t). \tag{C3}$$

2. Triangle

The triangular network studied here is depicted in Fig. 10(b). All containers C_1, C_2, and C_3 are connected to each other and therefore the rate equations describing the time evolution of $N_1(t)$, $N_2(t)$, and $N_3(t)$ have the same form. Equation (C4) is the rate equation that governs the dynamics in container C_1. The corresponding dynamical equations for $N_2(t)$ and $N_3(t)$ are obtained in the same way but are not written down here:

$$\dot{N}_1(t) = \frac{V_{d-1}(a_{21})}{V_d(R_2)}\int_0^t dt'\mathcal{N}_2(t')\sigma_{21}(t-t') + \frac{V_{d-1}(a_{31})}{V_d(R_3)}\int_0^t dt'\mathcal{N}_3(t')\sigma_{31}(t-t') - \frac{V_{d-1}(a_{12})}{V_d(R_1)}\int_0^t dt'\mathcal{N}_1(t')[\kappa_{12}(t-t')+\Delta_{12}(t-t')] - \frac{V_{d-1}(a_{13})}{V_d(R_1)}\int_0^t dt'\mathcal{N}_1(t')[\kappa_{13}(t-t')+\Delta_{13}(t-t')]. \tag{C4}$$

The behavior of $N_1(t)$, $N_2(t)$, and $N_3(t)$ is very sensitive to changes in the network structure. The response from these changes are not easily predicted by Eq. (C4). Instead Eq. (59) can be used to state a simplified version of Eq. (C4). Note that this equation only is valid in the large-time limit if the number of particles in the tubes is small. Applying Eq. (59) to container C_1 in the triangular network gives

$$\dot{N}_1(t) = \frac{V_{d-1}(a_{21})}{V_d(R_2)}\frac{D}{\ell_{21}}N_2(t) + \frac{V_{d-1}(a_{31})}{V_d(R_3)}\frac{D}{\ell_{31}}N_3(t) - \frac{D}{V_d(R_1)}\left[\frac{V_{d-1}(a_{12})}{\ell_{12}}+\frac{V_{d-1}(a_{13})}{\ell_{13}}\right]N_1(t). \tag{C5}$$

Corresponding first-order rate equations for $N_2(t)$ and $N_3(t)$ are found in the same way.

3. T network

The T-shaped network under investigation in this subsection is depicted in Fig. 10(c). Since all containers C_1, C_2, and C_3 are connected to container C_4 and not to each other, the rate equations governing the dynamics in C_1, C_2, and C_3—that is, $N_1(t)$, $N_2(t)$, and $N_3(t)$, respectively—all have a similar form

$$\dot{N}_i(t) = \frac{V_{d-1}(a_{4i})}{V_d(R_4)}\int_0^t dt'\mathcal{N}_4(t')\sigma_{4i}(t-t') - \frac{V_{d-1}(a_{i4})}{V_d(R_i)}\int_0^t dt'\mathcal{N}_i(t')[\kappa_{i4}(t-t')+\Delta_{i4}(t-t')], \quad i=1,2,3. \tag{C6}$$

The middle container C_4 has connections to all other containers C_1, C_2, and C_3. This leads to a rate equation for $N_4(t)$ of the form

$$\dot{N}_4(t) = \sum_{j=1}^{3} \frac{V_{d-1}(a_{j4})}{V_d(R_j)} \int_0^t dt' \mathcal{N}_j(t') \sigma_{j4}(t-t') - \frac{1}{V_d(R_4)} \int_0^t dt' \mathcal{N}_4(t') \times \sum_{j=1}^{3} V_d(a_{4j}) [\kappa_{4j}(t-t') + \Delta_{4j}(t-t')]. \quad \text{(C7)}$$

The rate equations derived in this subsection are used in the study of the junction, shown in Fig. 15.

APPENDIX D: ELIMINATION OF JUNCTIONS IN THE ASYMPTOTIC REGIME

The network studied in this section is a generalization of the one depicted in Fig. 15. Here, a junction having an arbitrary number of connections is studied and it will be demonstrated that the dynamical equations governing the transport in a system having junction points can be simplified in the large time limit. First, it will be shown that the current of particles in and out of a junction point eventually will balance each other out and that this occurs faster than the time it takes before an equilibrium particle distribution is attained throughout the network. This derives from the fact that the volume of the junction (proportional to a^d) is much smaller than the volumes of the containers (proportional to R_i^d, $i=1,\ldots,M$), where d is the dimensionality, a is the tube radius, and M is the number of containers. The tubes connecting the junction are assumed to have the same radius. Second, it will be demonstrated how to simplify the transport equations in such a way that the dynamical variable for the junction $N(t)$ can be eliminated completely. This might be desirable when working with large networks.

Consider a junction with dynamical behavior contained in $N_j(t)$ and volume $V_d(a)$ that has connections to M containers with volumes $V_d(R_i)$, $i=1,\ldots,M$. The equation governing the dynamics of the junction point written in Laplace space reads

$$sN_j(s) - N_j(0) = -sN_j(s)\frac{V_{d-1}(a)}{V_d(a)} \sum_{i=1}^{M} [\kappa_{ji}(s) + \Delta_{ji}(s)] + \sum_{i=1}^{M} sN_i(s)\frac{V_{d-1}(a)}{V_d(R_i)}\sigma_{ij}(s). \quad \text{(D1)}$$

This equation is a generalization of Eqs. (29) (see Sec. VI). The junction point studied here is such that $a \ll R_i$, and since

$$\frac{V_{d-1}(a)}{V_d(a)} = c_d \frac{1}{a}, \quad \frac{V_{d-1}(a)}{V_d(R_i)} = c_d \frac{1}{a}\left(\frac{a}{R_i}\right)^d, \quad \text{(D2)}$$

where

$$c_d = \frac{d}{d-1}\Gamma\left(\frac{d}{2}\right)\left[\Gamma\left(\frac{d-1}{2}\right)\right]^{-1}\pi^{-1/2}$$

(found by using the formula for a d-dimensional sphere; see Sec. II), the term proportional $(a/R_i)^d$ can be neglected and a closed expression for $N_j(s)$ can be obtained. Solving Eq. (D1) after eliminating the second term leads to

$$N_j(s) = \frac{N_j(0)}{s\left(1 + \frac{c_d}{a}\sum_{i=1}^{M}[\kappa_{ji}(s) + \Delta_{ji}(s)]\right)}. \quad \text{(D3)}$$

The inverse Laplace transform of $N_j(s)$ is a sum of exponentials,

$$N_j(t) = \sum_{p=1}^{\infty} \alpha_p e^{-\beta_p t}, \quad \text{(D4)}$$

where α_p is the residue of $N_j(s)$ at pole $s=-\beta_p$, $\beta_p \in \mathbb{R} > 0$. The poles are given by the zeros of

$$s + c_d \sum_{i=1}^{M} \frac{q_{ij} D_{ij}}{a\ell_{ij}} \frac{\cosh q_{ji}}{\sinh q_{ij}} = 0, \quad \text{(D5)}$$

where $q_{ij}^2 = s\ell_{ij}^2/D_{ij}$. When the currents in and out of the junction point balances each other out there is no accumulation of particles and $\dot{N}_j(t)=0$. This is easily verified from Eq. (D4) by evaluating the derivative in respect to t at $t=\infty$:

$$\frac{d}{dt}N_j(t) = \sum_{p=1}^{\infty} (-\beta_p)\alpha_p e^{-\beta_p t} \to 0 \quad \text{as } t \to \infty. \quad \text{(D6)}$$

Let τ_{junction} be an estimate of the time it takes until $\dot{N}_j(t)=0$. It is related to the decay exponents β_p [see Eqs. (38) and (43)] which are zeros of Eq. (D5). From Eq. (D5) it is clear that the zeros scales with $D/a\ell$ (it is assumed that $D_{ij} \sim D$ and $\ell_{ij} \sim \ell$) which leads to the estimate $\tau_{\text{junction}} \sim a\ell/D$. Let τ_{network} be an estimate of the time it takes to reach an overall equilibrium particle distribution in the network. As a rough estimate Eq. (50) can be used which was found for a two-node network. If the containers have volumes proportional to R^d, then

$$\tau_{\text{network}} \sim \frac{a\ell}{D}\left(\frac{R}{a}\right)^d.$$

If $R \gg a$, then $\tau_{\text{junction}} \ll \tau_{\text{network}}$. This is is supported by the numerical calculation shown in Fig. 16 where the curve corresponding to $N_4(t)$ flattens out relatively fast.

For networks where there are many junctions and containers involved it might be desirable to reduce the number of variables in the dynamical equations governing the particle transport. This can be done in the regime where $\dot{N}_j(t)=0$ is valid and Eq. (59) is applicable. Applying Eq. (59) for a junction point j having M connections and using $\dot{N}_j(t)=0$ leads to

$$0 = \sum_{i=1}^{M} \mathcal{C}_{ij} V_{d-1}(a) \frac{D_{ij}}{\ell_{ij}} \left[\frac{N_i(t)}{V_d(R_i)} - \frac{N_j(t)}{V_d(a)}\right]. \quad \text{(D7)}$$

In this way it is possible to express $N_j(t)$ in terms of $N_1(t),\ldots,N_M(t)$. Inserting the solution to this matrix equation in the dynamical equations eliminates the explicit dependence of $N_j(t)$. Equations (D8)–(D10) show this explicitly for the case of a three-way junction depicted in Fig. 15, where $N_4(t)$ has been taken away completely:

$$\dot{N}_1(t) = \frac{\ell_{24}D}{\ell^2}\frac{V_{d-1}(a)}{V_d(R_2)}N_2(t) + \frac{\ell_{34}D}{\ell^2}\frac{V_{d-1}(a)}{V_d(R_3)}N_3(t) - \frac{(\ell_{24}+\ell_{34})D}{\ell^2}\frac{V_{d-1}(a)}{V_d(R_1)}N_1(t), \tag{D8}$$

$$\dot{N}_2(t) = \frac{\ell_{14}D}{\ell^2}\frac{V_{d-1}(a)}{V_d(R_1)}N_1(t) + \frac{\ell_{34}D}{\ell^2}\frac{V_{d-1}(a)}{V_d(R_3)}N_3(t) - \frac{(\ell_{14}+\ell_{34})D}{\ell^2}\frac{V_{d-1}(a)}{V_d(R_2)}N_2(t), \tag{D9}$$

$$\dot{N}_3(t) = \frac{\ell_{14}D}{\ell^2}\frac{V_{d-1}(a)}{V_d(R_2)}N_1(t) + \frac{\ell_{24}}{\ell^2}\frac{V_{d-1}(a)}{V_d(R_2)}N_2(t) - \frac{(\ell_{14}+\ell_{24})D}{\ell^2}\frac{V_{d-1}(a)}{V_d(R_3)}N_3(t),$$

$$\ell^2 \equiv \ell_{14}\ell_{24} + \ell_{24}\ell_{34} + \ell_{14}\ell_{34}. \tag{D10}$$

[1] A. Karlsson, R. Karlsson, M. Karlsson, F. Ryttsén, and O. Orwar, Nature (London) **409**, 150 (2001).
[2] A. Karlsson, K. Sott, M. Markström, M. Davidson, Z. Konkoli, and O. Orwar, J. Phys. Chem. B **109**, 1609 (2005).
[3] M. Karlsson, M. Davidson, R. Karlsson, A. Karlsson, J. Bergenholtz, Z. Konkoli, A. Jesorka, T. Lobovkina, J. Hurtig, M. Voinova, and O. Orwar, Annu. Rev. Phys. Chem. **55**, 613 (2004).
[4] J. P. Laplante, M. Pemberton, A. Hjelmfelt, and J. Ross, J. Phys. Chem. **99**, 10063 (1995).
[5] A. Hjelmfelt and J. Ross, J. Phys. Chem. **97**, 7988 (1993).
[6] A. Hjelmfelt, F. W. Schneider, and J. Ross, Science **260**, 335 (1993).
[7] I. V. Grigoriev, Y. A. Makhnovskii, A. M. Berezhkovskii, and V. Y. Zitserman, J. Chem. Phys. **116**, 9574 (2002).
[8] A. M. Berezhkovskii and A. V. Barzykin, Chem. Phys. Lett. **383**, 6 (2004).
[9] L. Dagdug, A. M. Berezhkovskii, S. Y. Shvartsman, and G. H. Weiss, J. Chem. Phys. **119**, 12473 (2003).
[10] L. Dagdug, A. M. Berezhkovskii, and G. H. Weiss, Phys. Rev. E **69**, 012902 (2004).
[11] S. M. Bezrukov, A. M. Berezhkovskii, M. A. Pustovit, and A. Szabo, J. Chem. Phys. **113**, 8206 (2000).
[12] H. C. Berg and E. M. Purcell, Biophys. J. **20**, 193 (1977).
[13] M. A. Spiegel, *Schaum's Outline of Laplace Transforms* (Cambridge University Press, Cambridge, England, 1986).
[14] W. R. LePage, *Complex Variables and the Laplace Transform for Engineers* (Dover, New York, 1980).
[15] P. Stange, D. Zanette, A. Mikhlov, and B. Hess, Biophys. Chem. **79**, 233 (1999).
[16] W. H. Press, B. P. Flannery, A. S. Teukolsky, and W. T. Wetterling, *Numerical Recipes* (Cambridge University Press, New York, 1986).
[17] T. Bodineau and B. Derrida, Phys. Rev. Lett. **92**, 180601 (2004).
[18] R. Juhász, L. Santen, and F. Iglói, Phys. Rev. Lett. **94**, 010601 (2005).
[19] M. R. Evans, D. P. Foster, C. Godrèche, and D. Mukamel, Phys. Rev. Lett. **74**, 208 (1995).
[20] M. L. Simpson, G. S. Sayler, J. T. Fleming, and B. Applegate, Trends Biotechnol. **19**, 317 (2001).
[21] V. Krishnamurthy and E. V. Krishnamurthy, BioSystems **49**, 205 (1999).
[22] N. G. Rambidi, BioSystems **44**, 1 (1997).
[23] M. Conrad and K. P. Zauner, BioSystems **45**, 59 (1998).
[24] K. P. Zauner and M. Conrad, Soft Comput. **5**, 39 (2001).
[25] K. P. Zauner and M. Conrad, Naturwiss. **87**, 360 (2000).
[26] S. Ji, BioSystems **52**, 123 (1999).
[27] C. Siehs and B. Mayer, Nanotechnology **10**, 464 (1999).
[28] K. Akingbehin, BioSystems **35**, 223 (1995).
[29] K. Akingbehin and M. Conrad, J. Parallel Distrib. Comput. **6**, 245 (1989).
[30] M. Conrad, Eur. J. Oper. Res. **30**, 280 (1987).
[31] K. G. Kirby and M. Conrad, Physica D **22**, 205 (1986).
[32] K. G. Kirby and M. Conrad, Bull. Math. Biol. **46**, 765 (1984).
[33] R. Kampfner and M. Conrad, Bull. Math. Biol. **45**, 931 (1983).
[34] R. Kampfner and M. Conrad, Bull. Math. Biol. **45**, 969 (1983).
[35] B. Hess and M. Mikhailov, Science **264**, 223 (1994).
[36] D. J. Watts and S. H. Strogatz, Nature (London) **393**, 440 (1998).
[37] D. J. Watts, *Small Worlds: The Dynamics of Networks between Order and Randomness* (Princeton University, Princeton, 1999).
[38] L. M. Delves and J. L. Mohamed, *Computational Methods for Integral Equations* (Cambridge University Press, London, 1985).